Modeling the behaviour of sulfur in magmatic systems from source to surface: Application to Whakaari/White Island, Aotearoa New Zealand, and Etna, Italy

Ery C. Hughes: Te Pū Ao | GNS Science (e.hughes@gns.cri.nz)
Joseph Biasi: University of Wyoming
Isabel Fendley: University of Oxford
Kristen Rahilly: Oregon State University
Tyler Schlieder: Pacific Northwest National Laboratory
Heather Winslow: University of Nevada
Tobias P. Fischer: University of New Mexico
Paul Wallace: University of Oregon

This paper is a non-peer review pre-print submitted to EarthArXiv, which has been submitted to the Journal of Geological and Volcanology Research for peer review.

Twitter handles: @eryhughes, @izzifen, @kristen_rahilly, @HeatherBWinslow

Abstract

Our understanding of the role of volcanoes in the global sulfur cycle and how volcanic gas emissions can be used to monitor volcanoes is limited by the complex interactions between hydrothermal systems and volcanic sulfur emissions. Hydrothermal systems influence the amount and speciation of volcanogenic sulfur which is ultimately released to the surface/atmosphere via a range of physicochemical processes. To understand the effect of the hydrothermal system, including the presence of a crater lake, on surface emissions we model the magmatic-hydrothermal systems at Whakaari/White Island, Aotearoa New Zealand, and Etna, Italy. We quantify the magmatic sulfur inputs using mass balance and MELTS modelling (thermodynamic model of crystallisation); model the effects of degassing using D-Compress and SolEx (empirical models of melt-gas equilibria); and model the influence of the hydrothermal system using CHIM-XPT and EQ3/6 (thermodynamic and kinetic models of gas+water±rock reactions), which we compare to measured plume and fumarole compositions. We find that the sulfur inputs can broadly equal sulfur outputs over long timescales. However, the hydrothermal system can modulate the total mass of sulfur released and its H_2S/SO_2 ratio on shorter timescales, especially as the system evolves from water- to gas-dominated through the development of dry, gas-dominated pathways.

Keywords: sulfur, Whakaari, Etna, hydrothermal systems, degassing

1 Introduction

Volcanoes are a critical component of the global sulfur cycle; therefore, a robust understanding of the journey of sulfur through volcanic systems is needed (e.g., Kagoshima et al., 2015). However, the behavior of sulfur within magmatic systems from source (parent magma) to surface (outgassing) is difficult to constrain due to the wide range of potential oxidation states, species, and phases sulfur can be present in (e.g., Baker & Moretti, 2011, Moretti & Stefansson, 2020; Cicconi et al., 2020). In particular, the role of hydrothermal "scrubbing" in modulating the eventual output of sulfur at the surface is important to constrain (e.g., Symonds et al., 2001; de Moor et al., 2019; Christenson et al, 2017; Fischer et al., 2015). Following Symonds et al. (2001), we use a broad definition for "scrubbing", which refers to the removal of sulfur from volcanic gas through reactions with water±rock in the hydrothermal system (i.e., both hydrolysis of SO_2 to H_2S and precipitation of sulfur-bearing minerals).

Changes in the flux and composition of gases emitted at volcanoes are an integral part of volcano monitoring efforts as they are an indicator of magmatic input and can suggest increased likelihood of eruption (recent examples from: Werner et al., 2011; Patane et al., 2013; de Moor et al., 2016a; Aiuppa et al., 2017). The combination of absolute S and CO_2 fluxes with C/S ratios is particularly useful for interpreting the magmatic system because CO_2 and S fractionate during degassing and hydrothermal interactions. CO_2 is less soluble than S in silicate melts, causing CO_2 to exsolve into a gas phase at higher pressures than S (e.g., Shinohara et al., 2008; Lesne et al., 2011; Lopez et al., 2018). CO_2 is also less soluble than S in hydrothermal waters; hence, CO_2 does not react with hydrothermal waters, unlike S (e.g., Symonds et al., 2001; de Moor et al., 2016b). SO_2 is easily measured using ground- and space-based techniques due to its low background abundance in the atmosphere (e.g., Carn et al., 2017). The CO_2 flux can then be estimatted using the measured sulfur flux and C/S ratio of the gas (e.g., Allard 1991; Williams et al., 1992; Fischer et al., 2019).

Here we constrain sulfur inputs, outputs, and extent of hydrothermal scrubbing including the effects of shallow water scrubbing through the presence of a crater lake for two

volcanoes with active hydrothermal systems. Our approach for modeling sulfur from source to surface provides a quantitative assessment of the relative importance of the different processes affecting sulfur. We choose Whakaari/White Island, Aotearoa New Zealand (referred to as Whakaari throughout), and Etna, Italy, as case studies. Importantly, both have abundant published and/or freely accessible monitoring data on the flux and composition of the melt and gas within the volcanic systems. Comparing these volcanic systems allows us to evaluate the influence of a crater lake (present at Whakaari but absent at Etna) and also understand the effectiveness of our modeling approach for systems with different compositions and sub-surface architectures. We use these case studies to: (1) evaluate whether the sulfur flux at the surface can be balanced by the sulfur flux derived from the parent magma into the system, and (2) quantify how the presence of a hydrothermal system affects the sulfur emission at the surface.

Magmatic sulfur inputs were determined using a combination of whole-rock and melt-inclusion data; edifice volumes and ages; crystallisation modeling using MELTS (Asimow & Ghiorso 1998; Ghiorso et al. 2002); and using a range of intrusive to extrusive magma volume estimates. The process of degassing on melt and gas chemical composition was modelled using D-Compress (Burgisser et al. 2015) and SolEx (Witham et al. 2012). To model the effects of the hydrothermal system, we use EQ3/6 geochemical models (Wolery, 1992; Wolery and Daveler, 1992) and CHIM-XPT (Reed et al. 2016) to constrain the effects of scrubbing through hydrothermal systems of varying maturity, temperatures, and water chemistries. Sulfur outputs were compared to high and low temperature fumarole and plume compositions to evaluate the relative importance of different volcanic processes.

2 Geological setting

Whakaari:

Whakaari is Aotearoa New Zealand's most active volcano (see review by Kilgour et al., 2021), located ~50 km offshore of the North Island in the Bay of Plenty (Figure 1a). It is at the north end of the Taupō Volcanic Zone, which is a rifted arc caused by oblique, westward subduction of the Pacific plate under the Australian plate (Cole, 1990; Wallace et al., 2004). The volcano sits on continental crust and is mostly composed of andesitic to dacitic magmas, with occasional high-Mg andesites (e.g., Cole et al., 2000). The magmas are relatively H_2O-poor, with <1.5 wt% H_2O recorded in melt inclusions and from plagioclase hygrometry (Wardell et al., 2001; Rapien et al., 2003; Esposito et al., 2014; Mandon et al., 2021; Kilgour et al., 2021). Degassing is primarily passive (i.e., non-eruptive) and occurs through vents within the main crater, distributed fumaroles on the broader crater floor, and diffuse degassing (e.g., Wardell et al., 2001). There is an active hydrothermal system and the main crater periodically infills with a lake (e.g., Christenson et al., 2017; Kilgour et al., 2021). The composition of hydrothermal waters is either seawater, brine, and/or mixtures of seawater, brine, and meteoric water (Giggenbach et al., 2003; Christenson et al., 2017). Hydrothermal fluids may circulate to a depth of ~1 km, whereas a two-phase (gas + fluid) system occurs at shallower levels (Jolly et al., 2017). Permeabilities throughout the hydrothermal system vary widely depending on localized fracturing, dissolution, or mineral precipitation (Heap et al., 2017). Between 2005–2015, 127 ± 71 t/d S was emitted during passive degassing using a combination of space-based and ground-based measurements (Fischer et al., 2019). The GeoNet program regularly monitors the volcano which, prior to the 2019 eruption, included on-the-ground measurements of fumarole temperatures and compositions; crater lake height and temperature; and ground deformation. Since 2019, on-the-ground monitoring has not been undertaken and real-time

seismo-acoustic monitoring has degraded gradually. At the time of writing, (as of June 2023) all on-the-ground monitoring is no longer operational. Airborne measurements of SO_2, H_2S, and CO_2 flux from the plume, plus observation flights are continuing. All monitoring data for Whakaari are freely available from the GeoNet website (https://www.geonet.org.nz/).

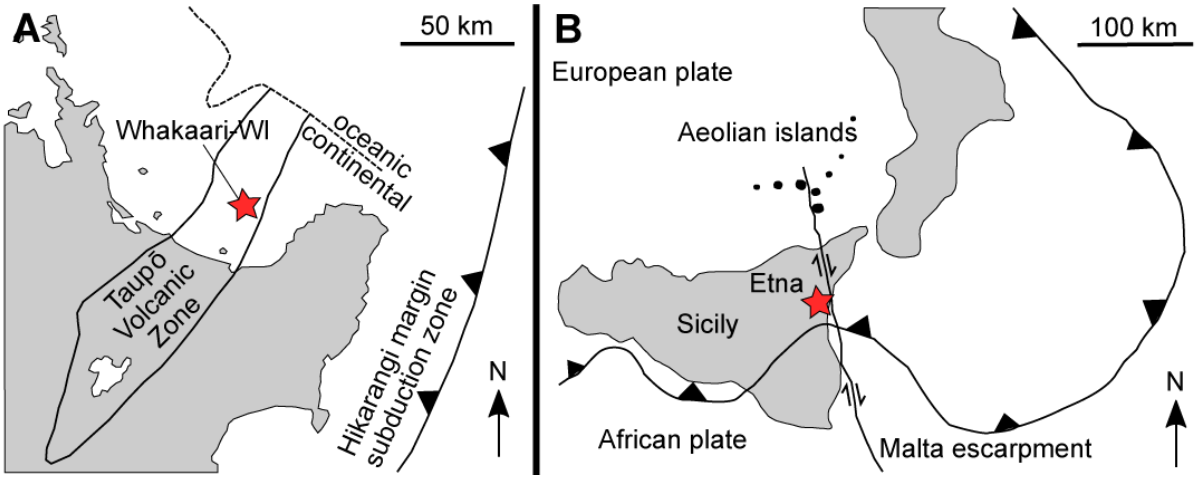

Figure 1 Location and simplified tectonic setting of the two volcanoes chosen for this study: **(a)** Whakaari/White Island (WI), Aotearoa New Zealand, and **(b)** Etna, Italy. Modified from Cole et al. (2000) and Kahl et al. (2015), respectively.

Etna:

Etna is one of the most active basaltic volcanoes in the world and is located on the island of Sicily, Italy (Figure 1b). It occurs at the intersection between the Aeolian arc (related to the collision of the African and European plates) and the Malta escarpment (e.g., Barberi et al., 1974). The magma composition is intermediate between ocean island and island arc basalts (e.g., Schiano et al., 2001). The eruption style at Etna is highly varied (effusive lava flows to explosive Plinian eruptions), and erupted magmas are often volatile-rich (e.g., Coltelli et al., 1998; Metrich et al., 2004; Burton et al., 2005). The volcano is persistently degassing from multiple summit vents through many fumaroles and extensive diffuse flank degassing (e.g., Aiuppa et al., 2006; Allard et al., 2006; Hernández et al., 2015). Etna emitted 1052 ± 532 t/d S both passively (using data between 2005–2015) and during eruptions (using data between 2005–2017) using space and ground-based measurements (Fischer et al., 2019). The extent of the hydrothermal system present at Etna is smaller than that at Whakaari and is characterized by small-scale, shallow pockets of mostly meteoric hydrothermal fluids near active vents, as well as the likely presence of deeper hydrothermal brines (Brusca et al., 2001; Behnke et al., 2008). Based on thermochemical modeling, Liotta et al. (2010) report that the conversion of SO_2 into H_2S happens rapidly as exsolved magmatic gas cools from 1150 to 400 °C, resulting in molar SO_2/H_2S between 1 and 5. Partial dissolution of SO_2 and H_2S occurs as gases intersect unsealed fractures filled with near boiling water of an uncertain, but likely meteoric, origin at high-pressures (>50 bars) and high-temperatures (>260 °C). At shallower pressures, the interactions between hydrothermal fluids and ascending gases occur too rapidly for efficient scrubbing (i.e., dissolution into H_2O) of SO_2 (Giammanco et al., 1998; Liotta et al., 2010).

3 Methods

We model the flux and composition of volatile components from when they are dissolved in the initial melt to emission at the surface including the effects of crystallisation, degassing, and water-gas-rock reactions (Figure 2). By comparing the modeled and measured volatile flux and

composition at different stages within the volcanic system, we can evaluate which processes are occurring and their relative importance. Compositional input data to the various models, as well as measured gas flux and fumarole and plume compositions, are given in the Supplementary Material for Whakaari and Etna.

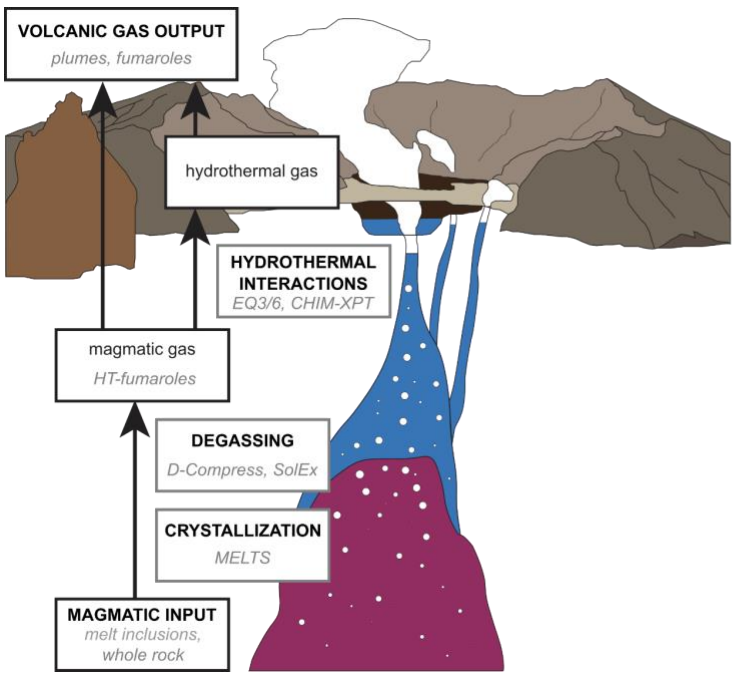

	WHAKAARI	ETNA
VOLCANIC GAS OUTPUT *(measurements)*		
S flux (t/d)	127 ± 71	1052 ± 532
C/S	4.0	6.7
HYDROTHERMAL INTERACTIONS *(EQ3/6 and CHIM-XPT)*		
pressure (bars)	1–40	5–100
temperature (°C)	58–400	90–300
initial CO_2/SO_2	1–5	1–12
DEGASSING	*(D-Compress)*	*(SolEx)*
pressure (bars)	<1500	<1500
temperature (°C)	1050–1200	1150
initial H_2O (wt%)	1.0–4.0	1.0–3.6
initial CO_2 (ppm)	10–1270	500–4100
initial S (ppm)	~100–2500	500–3500
CRYSTALLIZATION *(MELTS)*		
pressure (bars)	1500–2000	500–2000
oxygen fugacity (ΔNNO)	0	0.5
Vapor-saturated?	yes	yes
Crystallisation (%)	25	67
MAGMATIC INPUT		
intrusive:extrusive (volume)	1:1–10:1	1:1–10:1
initial S (ppm)	2430	4630
S flux (t/d)	92–762	75–9370

inputs (italic), outputs/measurements (normal)

Figure 2. *(left)* Schematic illustration showing our approach to modeling sulfur in the magmatic-hydrothermal systems of both Whakaari and Etna (illustration: Whakaari). Reservoirs of sulfur are shown in black outlined boxes, with observables of these reservoirs shown in *grey italics*. Processes affecting sulfur as it moves between reservoirs are shown in boxes outlined in grey, where the program used to model this process is shown in *grey italics*. *(right)* Table indicating the processes considered in our approach (**black bold**) including: programs used for modelling (*grey italics*), inputs used for the models (*italics*), outputs and best-fit solutions (normal), and measurements made at the volcanoes (normal) for Whakaari (left, blue) and Etna (right, red).

3.1 Magmatic input and crystallisation

To quantify the sulfur inputs into the volcanic-hydrothermal systems at Whakaari and Etna, we assume that the only sulfur input is mantle-derived sulfur from the primary magma (i.e., there is no addition of crustal material). To calculate the sulfur input we require an estimate of: (1) the initial concentration of sulfur in primary magmas, and (2) the primary magma flux from the mantle.

The sulfur content of the mantle-derived parent melt is a function of the amount of sulfide- and/or sulfate in the mantle, which depends on the sulfur content and oxygen fugacity of the mantle source, and the extent of mantle melting (e.g., Ding & Dasgupta, 2018; Chowdhury & Dasgupta, 2019). At low degrees of partial melting, there is still sulfate and/or sulfide sources in the mantle after partial melting and the sulfur content of the mantle-derived melt is governed by the sulfur content at anhydrite saturation (S^TCAS) or sulfide saturation (S^TCSS). At high degrees of partial melting, when both sulfide and sulfate have been exhausted, the sulfur content of the melt is governed by the amount of sulfide and/or sulfate initially present, which is then diluted as more melt is generated. As both volcanoes are in subduction

zone settings, our estimate of initial sulfur content of the mantle is affected by uncertainty in the contribution from the subducting slab and the degree of partial melting. Therefore, our best estimate of the initial sulfur concentration of the primary magma is the highest measured sulfur concentration from primitive melt inclusions. Also, as sulfur degassing occurs mainly at shallow depths (lower pressures), melt inclusions trapped at higher pressure, deep in the system, should record sulfur concentrations more representative of the initial concentration in the melt (e.g., Wallace & Edmonds, 2011). We compiled melt inclusion data from Whakaari (Rapien et al., 2003; Wardell et al., 2001; Esposito et al., 2014; Mandon et al., 2021; Kilgour et al., 2021) and Etna eruptions between 2001–2016 (Metrich et al., 2004; Spilliaert et al., 2006; Collins et al., 2009; Schiavi et al., 2015; Gennaro et al., 2019; Edwards & Pioli, 2019; Potter et al., 2019). Measured sulfur concentrations are as much as 2430 and 4630 ppm in Whakaari and Etna, respectively, and we use these values as the starting values for petrogenetic modeling (full dataset available in the Supplementary Material).

We constrain the parental magma flux into the system using estimates of the time period over which a certain volume of primary magma entered the system. Both time and volume are challenging to constrain. Estimating the volume of magma which enters the system requires knowledge of both the intruded and extruded magma volumes, where I:E is the ratio of intrusive to extrusive magma volumes.

The extruded magma volume (and flux) can be estimated from observed volumes of erupted magma over a known time interval. For Whakaari, we used the edifice volume as the extruded magma volume (78 km^3; Duncan 1970; Cole et al., 2000) and the total edifice age (10 to 21 kyrs; Rapien et al., 2003; Shane et al., 2006). We note that the edifice volume used here is likely a minimum considering post-eruptive surface processes (e.g., edifice collapse and destruction) have likely removed an unknown volume of material from the current edifice over time. For Etna we used two different approaches: (1) total estimated eruptive volume during the lifetime of the volcano (350 km^3 over ~500 kyrs, Tanguy et al. 1997); and (2) directly calculated eruptive volumes during observed eruptions between 1970–2010 (Harris et al., 2011).

The intruded magma volume is more difficult to constrain due to lack of direct observations. A minimum estimate comes from the amount of crystallisation of the primary magma prior to eruption required to produce the composition of the erupted material calculating using MELTS modeling (Ghiorso & Sack 1995; Asimow & Ghiorso 1998). As for initial sulfur concentrations, attempting to estimate primary, mantle-derived melt compositions that fed each system requires certain assumptions and extrapolations. We assumed that the most primitive lavas were representative of the 'primary' magma compositions in both volcanic systems. A grid-search through a range of parameters (1300–700 °C temperature, relative oxygen fugacity (ΔNNO) of -3 to +3, 0–10 kbar pressure, and 0 wt% to H_2O-saturated conditions) during fractional crystallisation was used to find a liquid line of descent that would best match measured whole rock compositions. The best match was evaluated using least-squares residuals to measured MgO, CaO, Al_2O_3, and SiO_2 bulk rock data, which are most sensitive to the changes in these conditions. MELTS continuously tracks the mass of residual melt during fractional crystallisation, allowing us to correct for the mass of crystals removed from each system due to fractional crystallisation, and by extension, to estimate the mass of parent (least evolved) magma contributing to the total sulfur budget for each system. Combining the observed extruded magma volume with a calculated intruded magma volume from MELTS modelling gives a minimum I:E ratio.

However, some magma intruded in the crust may not have contributed to erupted magma at the surface. Therefore, the maximum estimate of the primary magma flux (and therefore S flux) depends on the maximum I:E assumed. Excess SO_2 flux measurements at

volcanoes (i.e., more SO_2 emitted than be derived from the erupted magma) are typically used to constrain I:E (e.g., Steffke et al., 2011). Thus, using empirically constrained I:E at Whakaari or Etna to estimate the S flux would lead to circular arguments. We therefore conducted a series of calculations for both systems using I:E up to 10:1 (these are reasonable ratios proposed for other systems; Steffke et al., 2011) to better quantify the effect of residual unerupted magma on estimated S flux.

3.3 Degassing: D-Compress and SolEx

We used two degassing models to simulate degassing of typical Whakaari and Etna magmas as they ascend through the upper crust (<1500 bar): D-Compress (Burgisser et al., 2015) and SolEx (Witham et al., 2012). We compare the observed gas compositions measured at fumaroles and plumes to the calculated compositions during the degassing paths. This approach provides insight on the initial volatile contents of the melt (which are key constraints on the sulfur input calculations through mass balance); the pressure at which the gas may have separated from the magma; and whether the observed gas compositions emitted at the surface can be generated by degassing or require the influence of the hydrothermal system.

Both models predict the equilibrium melt and vapour compositions for multi-volatile systems (CO_2, H_2O, S, and additionally Cl for SolEx) under closed- and open-system degassing conditions. Although in both models, the solubility of CO_2 and H_2O in the melt is related to the fugacity of these species in the gas phase, the models' treatment of sulfur is very different. D-Compress relates the solubility of H_2S and SO_2 in the melt to the fugacities of these species in the gas phase, whereas SolEx treats sulfur as a trace element that partitions into the gas phase. Both are based on empirical calibrations that, especially for sulfur, limit the conditions that are appropriate due to a lack of experimental data. The total sulfur in the system cannot be specified in D-Compress, which instead calculates the total sulfur concentration in the melt that saturates the melt in a gas phase at the chosen initial conditions. We were not able to recreate the high initial sulfur content found in melt inclusions from Etna, hence we only applied D-Compress to modeling degassing at Whakaari. Conversely, SolEx is only calibrated for basaltic melts (Stromboli- and Masaya-like melt compositions) at high oxygen fugacities (f_{O2} > ΔNNO+0.5), hence we only use the model to simulate the behaviour at Etna, which has a similar composition to the calibration dataset and is relatively oxidised (ΔQFM = +1.2, Gaborieau et al., 2020).

For modeling Whakaari using D-Compress, we investigated a range of compositions and temperatures at different depths to simulate potential degassing scenarios from what are likely complexly configured magma storage zones beneath the volcano: basaltic andesite at 1200 °C and an initial pressure of 3000 bars; andesite at 1100 °C and 2000 bars; and dacite at 1050 °C and 1000–2000 bars. We used both the pre-defined basalt and rhyolite volatile solubility constants, as andesitic solubility constants are not available in D-Compress. All models were run under closed-system degassing conditions with 1–4 wt% H_2O and 10–1270 ppm CO_2 initially in the melt, and 0.01–1 wt% initial gas, which resulted in ~100–2500 ppm S initially in the melt. The CO_2 content was iterated until the approximate S content of Whakaari melt inclusions was obtained. Full details of the inputs for these simulations are given in the Supplementary Material.

For modeling Etna using SolEx, the melt composition chosen was the most primitive melt inclusion (lowest SiO_2) from the 2001–2003 eruptions at Etna (Gennaro et al., 2019) at 1150 °C and ΔNNO+0.5. Degassing style (closed vs. open) and initial volatile content (1.0–3.6 wt% H_2O, 500–4100 ppm CO_2, 500–3500 ppm S, and Cl was kept constant at 3500 ppm) were varied to see their effect on the vapor composition during degassing. The speciation of S in the vapor (i.e., mole fraction SO_2 and H_2S in the vapor) was calculated from the x_{ST} output

from SolEx using homogeneous vapour equilibrium. Full details of the inputs for these simulations and the S speciation calculations are given in the Supplementary Material.

3.4 Hydrothermal interactions: EQ3/6 and CHIM-XPT

Our approach follows the work of Di Napoli et al. (2016) using the EQ3/6 geochemical modeling software within the Enabling Knowledge Integration (ENKI) (http://enki-portal.org/) server through the Jupyter Notebooks open-source web application. We use the jus.R60 thermodynamic database with a maximum temperature of 350 °C and pressure of 165.2 bars. An initial packet of bulk magmatic gas (compositions taken from high-temperature fumaroles) is titrated into, and allowed to equilibrate at different temperatures and pressures, with a system consisting of bulk bedrock and various water compositions set to represent a hydrothermal system. The output composition of gas phase components is recorded after titration and equilibration with the water-rock system at the indicated pressure and temperature regime. All models were run in the 'relative rates' mode using the transition state theory rate law to model irreversible reactions between the minerals and waters (Wolery, 1992; Wolery and Daveler, 1992). Inputs into EQ3/6 are given in the Supplementary Material. Note that the EQ3/6 input did not allow for definition of H_2O (gas) as a titrant: therefore, our input magmatic gases are defined solely based on CO_2 and SO_2 molar ratios.

At Whakaari, we performed four to nine total runs for each water composition-pressure-temperature regime, with each step within a run using the water output from the previous step and the same initial magmatic gas composition. The generalized bulk rock composition used was the Whakaari central cone dacite from Cole et al. (2000). The initial magmatic gas packet was assumed to be the composition of high-temperature fumaroles with CO_2/SO_2 = 5 (Giggenbach et al., 1975) and was titrated through four different water compositions: brine (Christenson et al., 2017), seawater (McCollom, 2007), meteoric water (Berner and Berner, 2012; Hao et al., 2017), and Whakaari lake water (Christenson et al., 2017).

For Etna, we performed five total model runs for each water composition-pressure-temperature regime, with each step using the water output from the previous step and the same initial magmatic gas composition. Likely temperatures and pressures of the Etna hydrothermal system were used from Giammanco et al., (1998). We define a magmatic gas input of CO_2/SO_2 = 12 based on a multigas measurement by Aiuppa et al. (2008), taken when CO_2 flux was highest during the pre-eruptive period (CO_2 = 19062 t/d, SO_2 = 1631 t/d, H_2O = 13257 t/d). Generalised bulk rock composition used was K-trachybasalt (Giuffrida & Viccaro, 2017). Finally, we used an initial deep brine composition from sample 19 of Brusca et al. (2001) and a meteoric water composition from Berner and Berner (2012).

To characterize the effect water has on sulfur flux through hydrothermal systems, we used the program CHIM-XPT (formerly known as CHILLER; Reed et al. 2016). CHIM-XPT has the capability to compute reaction processes in water-rock-gas systems. Reaction processes can be calculated under changing composition, pressure, and temperature. CHIM-XPT modelling is restricted to pressures <5000 bar and temperatures <600°C. For our purpose, we titrated gas of a specific composition through water in order to see the output gas composition and concentration. This was done to test the effect of scrubbing on gases titrated through the hydrothermal system at Whakaari.

Input gas compositions came from high-temperature fumaroles (Giggenbach, 1987), which were used as a proxy for gases sourced from the underlying magma. We chose specific water geochemistry of samples collected from hot springs located in the crater (Giggenbach, 1987) as a best representative for the composition of the hydrothermal system. The models were run at 250 °C and 40 bars based on previous characterizations of Whakaari's

hydrothermal system (e.g., Giggenbach, 1987, 2003). CHIM-XPT bases its calculations on 1 kg of water and outputs a water/gas ratio (w/g) that can be scaled to larger volumes. We tested the evolution of a hydrothermal system by titrating increasing amounts of gas into the system and tracking changes in output gas composition. These observations can also be used to make predictions about gas composition and transfer related to the maturity of hydrothermal systems. High water/gas ratios (w/g) imply efficient gas scrubbing, typically associated with immature systems, which predictably alters gas compositions by effectively removing most of the amount of SO_2 present. Low w/g represents a mature system that is no longer able to efficiently scrub SO_2. In this context, a mature system with a low w/g implies the hydrothermal system is oversaturated with volatiles and at a high enough temperature to allow SO_2 to pass through the hydrothermal system relatively unaffected, thus no longer causing a scrubbing effect (Table 4). Inputs to CHIM-XPT are given in the Supplementary Material.

4 Results

4.1 Calculated magmatic input vs. surface emissions

At Whakaari, the best fit to whole-rock data using MELTS modeling is found under isobaric (1500–2000 bars) fractional crystallization at water-saturated conditions and a relative oxygen fugacity of ΔNNO=0 (where ΔNNO is the Ni-NiO buffer) (Figure 5a and b). The most evolved compositions were reproduced by MELTS after ~25% crystallization of the parent magma (I:E = 1:3). At Etna, the best fit is found with fractional crystallisation at water-saturated conditions at shallower (~500 bars) isobaric pressures and slightly more oxidised conditions (NNO+0.5) (Figure 5c and d). Good fits can also be found at ~2000 bars under similar conditions. The most evolved compositions require more extensive crystallisation (~67%) of the parent magma (I:E = 2:1). In both cases, these conditions closely match inferred conditions from other petrologic and geophysical methods (e.g., Whakaari: Cole et al. 2000, Etna: Cannata et al. 2018; Cashman & Edmonds, 2019).

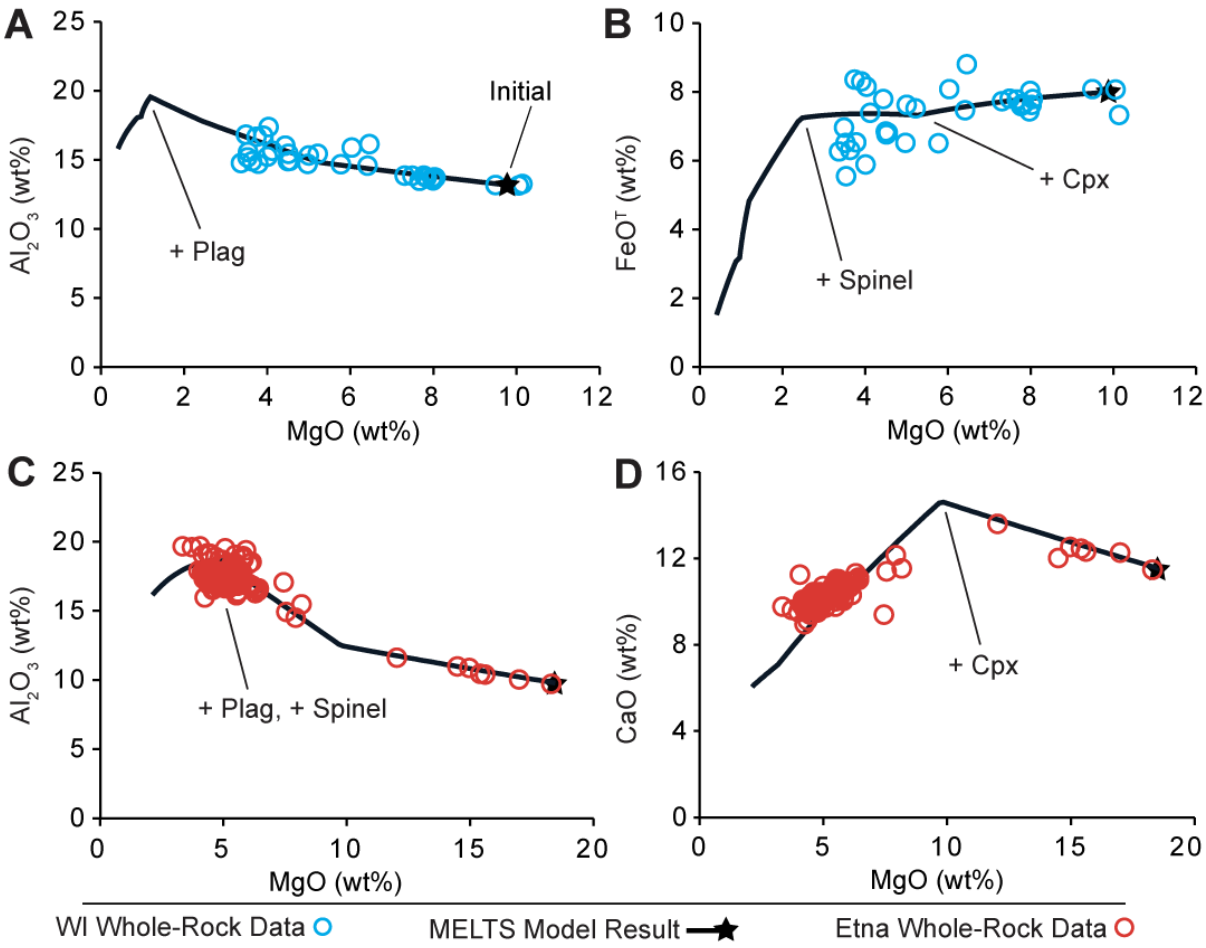

Figure 5 Results of MELTS modeling for **(a–b)** Whakaari (blue) with best fit parameters of isobaric fractional crystallization at 1500 bars, ΔNNO=0, and H_2O-saturated; and **(c–d)** Etna with best fit parameters of isobaric fractional crystallization at 500 bars, ΔNNO+0.5, and H_2O-saturated. Whole rock data is shown by open symbols and MELTS modelling results by the black line, where the starting composition is shown by the black star. Data from Armienti et al. (1989); Tonarini et al. (1995); Cole et al. (2000); Corsaro et al. (2007); Kamenetsky et al. (2007); Heyworth et al. (2007); Viccaro and Cristofolini (2008); Correale et al. (2014); Viccaro et al. (2015); Gennaro et al. (2019); Di Renzo et al. (2019).

For Whakaari, our estimate for surface gas emissions is 92–762 t/d S (I:E = 1:3 to 10:1), whereas the measured flux between 1983–2019 varies by two orders of magnitude (~3–900 t/d S; www.geonet.org.nz, Christensen et al., 2017), with an average of 127 ± 71 t/d S between 2005–2015 (Fischer et al., 2019) (Figure 6a). The wide range of estimated sulfur flux is due to uncertainty in the primary magma flux into the system (e.g., edifice age and volume, I:E). The minimum estimated flux based on intruded magma volume calculated using MELTS modelling is on the low end of measured flux values, but within error of the average flux between 2005–2015. The flux using an I:E = 1:1 is greater than the upper bound of 2005–2015 average.

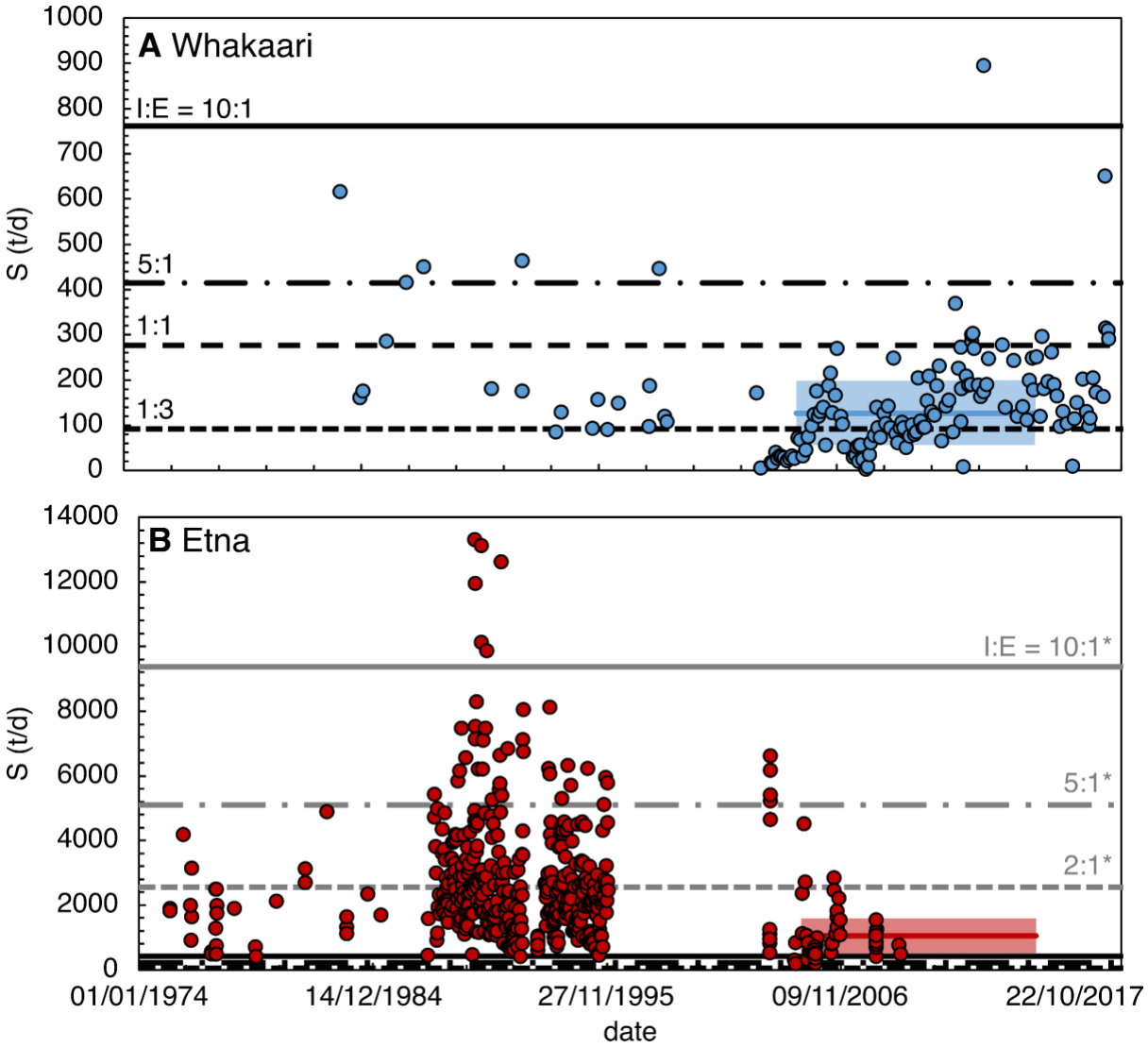

Figure 6 Sulfur flux (t/d S) for **(a)** Whakaari and **(b)** Etna: circles are measured values (Whakaari references: www.geonet.org.nz; Christensen et al., 2017. Etna references: Aiuppa et al., 2006, 2007 2008; Allard et al., 1991; La Spina et al., 2010; Salerno et al., 2009; Edner et al., 1994; Pugnaghi et al., 2006; Caltabiano et al., 1994; Bruno et al., 1999); the coloured box with the horizontal line (mean ± 1 standard deviation) represents the average output for 2005–2015 from Fischer et al. (2019); the horizontal lines are calculated using our minimum I:E from MELTS modeling of 1:3 or 2:1 (dot), 1:1 (dash: Whakaari only) 5:1 (dot dash), and 10:1 (solid), where black lines (both Whakaari and Etna) use edifice volume and age to calculate eruption rates and grey lines (only Etna and indicated with a *) use observed eruption rates.

For Etna, our estimate is 75–9370 t/d S using I:E = 2:1 to 10:1 and extruded volumes based on edifice volume to observed rates (Figure 6b). The measured values range from 200 to 13300 t/d S (Aiuppa et al., 2006, 2007, 2008; Allard et al., 1991; La Spina et al., 2010; Salerno et al., 2009; Edner et al., 1994; Pugnaghi et al., 2006; Caltabiano et al., 1994; Bruno et al., 1999), with an average between 2005–2015 of 1052±532 t/d S (Fischer et al., 2019) (Figure 6b). Our minimum estimate (75 t/d S), derived from a long term erupted volume of ~350 km^3, edifice age of ~500 kyrs (Tanguy et al., 1997), and I:E = 2:1, is approximately an order of magnitude lower than the average measured flux. The maximum estimate (9370 t/d S) uses historical erupted volume data from 1970–2010 (Harris et al., 2011) and I:E = 10:1, and is an order of magnitude larger than the average measure flux. The constraints on eruptive volume are more robust for the recent period (1970–2010) because of improved observations and

monitoring of recent eruptions (Harris et al., 2011). Our modeling indicates that it is possible to balance the observed sulfur output at Etna if I:E < 2:1 for flux measurements since ~2003 and closer to 2:1 to 5:1 for older measurements.

4.4 Magmatic gas compositions

Figure 7 examines the relationship between the outputs of D-Compress (Whakaari), SolEx (Etna), EQ3/6 (Whakaari and Etna), and CHIM-XPT (Whakaari) with measured fumarole and plume compositions. Filled black symbols are data measured from fumaroles at high temperatures for diamonds or low temperatures for squares (high *T* is >400 °C for Whakaari or >300 °C for Etna). At Whakaari, fumarole compositions are generally H_2O-rich, with higher temperature fumaroles being broadly richer in total sulfur (S_T) (Figure 7a). Both SO_2 and H_2S occur in the fumaroles (there is no systematic difference between high and low *T* fumaroles) but only SO_2 is present in the plume: molar SO_2/H_2S ratios range from 0 to 17.2, with an average of 5.4 ± 5.2 (Figure 7b). At Etna, fumarole compositions are poor in H_2O compared to Whakaari (Figure 7c). The SO_2/H_2S ratios for fumarole and plume compositions at Etna are highly variable, with SO_2/H_2S between 0.4 to 215 (Figure 7c).

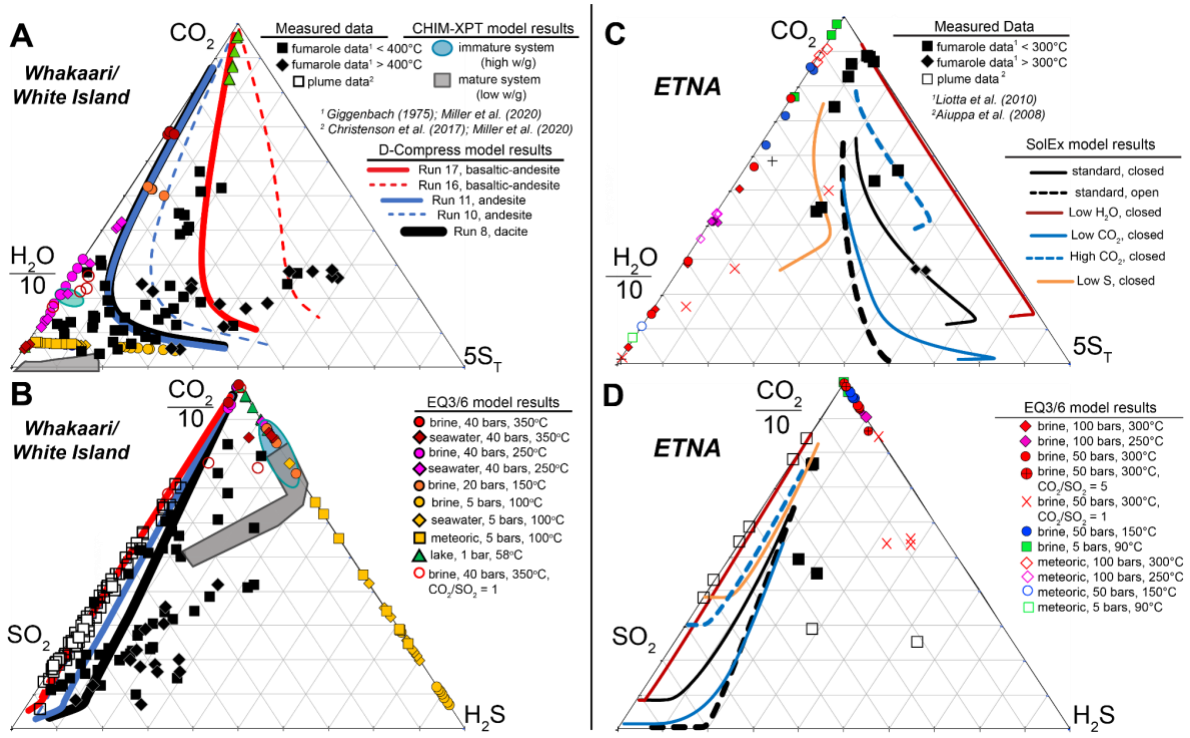

Figure 7 Gas composition for Whakaari and Etna plotted on ternary diagrams for **(a)** CO_2-H_2O-S_T and **(b)** CO_2-H_2S-SO_2. For Whakaari, model results are from D-Compress (curves), EQ3/6 (coloured symbols: initial magmatic CO_2/SO_2 = 5 unless otherwise noted), and CHIM-XPT (blue and grey filled regions), compared to fumarole and plume data (black filled and outlined squares: Giggenbach, 1975; Christenson et al., 2017; Miller et al., 2020). For Etna, model results from SolEx (curves) and EQ3/6 (coloured symbols: initial magmatic CO_2/SO_2 = 12 unless otherwise noted), compared to fumarole and plume data (black filled and outlined squares: Aiuppa et al., 2008; Liotta et al., 2010).

4.5 Degassing: D-Compress and SolEx

Results from degassing models are shown using solid and dashed curves in Figure 7 (D-compress for Whakaari and SolEx for Etna). Both models predict decreasing CO_2 mole fraction in the vapor with decreasing pressure (curves start close to the CO_2 apex in Figure 7a and c and move towards the H_2O-S_T edge with decreasing *P*). At low *P*, SolEx predicts the gas becomes more H_2O-rich and S-poor, whereas D-compress predicts the opposite (Figure 7a and c). Both models suggest the gas is SO_2-rich relative to H_2S, with increasing mole fractions of SO_2 at low *P* (Figure 7b and d).

For Whakaari, the D-Compress model produces gas compositions similar to measured plume and fumarole composition for initial conditions that had lower H_2O (<2 wt%) and gas mass fractions (0.01 wt%) compared to other runs with the same melt compositions, suggesting low initial volatile contents dissolved in the magma (Figure 7; dacite run 8, andesite 10 and 11, basaltic andesite 16 and 17: rhyolite models did not intersect measured compositions). For the dacite and basaltic andesite compositions, higher initial CO_2 concentrations better reproduced the measured gas compositions, whereas for the andesite composition, lower initial CO_2 concentrations were more appropriate. Basaltic andesite melt compositions produce more S-rich but H_2O-poor gas compositions in comparison to dacite and andesite melt (Figure 7a), but similar SO_2/H_2S ratios in all cases (Figure 7b).

For Etna using SolEx, open-system degassing produces more H_2O-rich gas compositions, with higher CO_2/S_T ratios at high *P* and lower CO_2/S_T ratios at low *P*, than closed-system degassing (Figure 7c). Decreasing initial H_2O or S results in higher CO_2/S_T ratios at all *P*, but more S-rich or H_2O-rich compositions, respectively, whereas decreasing initial CO_2 results in lower CO_2/S_T at all *P* (Figure 7c).

Both the D-Compress and SolEx model results intersect measured fumarole and plume compositions for Whakaari and Etna (Figure 7). At Whakaari, the D-Compress results recreate the ratio of CO_2/S_T of the fumarole data (Figure 7a); however, modeled gas outputs have higher SO_2/H_2S than fumarole compositions but similar to plume compositions (Figure 7b). These gas compositions are produced at 150–650 bars. The SolEx modeled results for Etna show a similar trend, recreating the CO_2/S_T of measured data but not the wider range of SO_2/H_2S values. These gas compositions are produced at 1000–1500 bars for the standard closed/open-system and low CO_2 calculations, but at 500 bars for low H_2O and S, but high CO_2, calculations.

4.5 Hydrothermal interactions: EQ3/6

The EQ3/6 gas data in Figure 7 are the compositions of the magmatic gas outputs after titrating through, and equilibrating with, hydrothermal waters of various compositions at a range of temperatures and pressures. Each temperature, pressure, and water chemistry condition has multiple resulting gas outputs (and hence multiple occurrences of the same symbols in Figure 7) as the water chemistry evolves. At Whakaari, nearly all of the modeled gas outputs have compositions with low total sulfur (Figure 7a) and very high H_2S relative to SO_2 (Figure 7b) compared to the observed fumarole gas compositions. In an attempt to increase the SO_2/H_2S ratio of modeled surface gas emissions, we increased the amount of SO_2 in our initial magmatic gas compositions to $CO_2/SO_2 = 1$ and titrated it through brine at 350 °C and 40 bars (red outlined circles). This magmatic gas input with a higher concentration of SO_2 is the only modeled gas that plots closer to the region of measured gas compositions in Figure 7B but still has too low of a SO_2 concentration than most fumarole and plume measurements.

None of the modeled gas outputs from EQ3/6 intersect compositions of measured gas from Etna, as they are too S-poor (Figure 7c and d). We increased the amount of SO_2 in our initial magmatic gas compositions to $CO_2/SO_2 = 5$ (red circles with cross in Figure 7c, 8d) and $CO_2/SO_2 = 1$ (X symbols in Figure 7c and d) to test the effects of more SO_2-rich magmatic gas

compositions entering the hydrothermal system. Only the models with $CO_2/SO_2 = 1$ have closer to the S_T of measured compositions (Figure 7c). Similar to Whakaari (Figure 7b), all EQ3/6 modeled output gases are too rich in H_2S relative to SO_2 (Figure 7d) when initial gas inputs are forced to equilibrate through hydrothermal water. The interactions modeled by EQ3/6 where all of the magmatic SO_2 is forced to interact with hydrothermal waters do not represent the measurements at either Whakaari or Etna, suggesting both volcanoes emit SO_2 through pathways with limited hydrothermal interaction.

4.6 Hydrothermal interactions: CHIM-XPT

CHIM-XPT produces output gas compositions after experiencing water-gas interactions which can ultimately be a reflection of hydrothermal system maturity. We progressively input gas into Whakaari's hydrothermal system to test changes in output gas chemistry as the w/g ratio decreases (note we did not apply CHIM-XPT to Etna). Initially, output gas shows an increase in H_2S/SO_2 followed by a drastic decrease (Figure 8a). An increase in H_2S/SO_2 is the direct result of hydrous interactions. SO_2 is consumed by hydrolysis reactions and produces H_2S (one form of scrubbing), thus initially increasing the H_2S/SO_2 ratio (Giggenbach, 1987). As more gas is titrated through the system, the SO_2 consumption decreases and scrubbing becomes inefficient causing the H_2S/SO_2 ratio of surface gas emissions to decrease (Figure 8a). This decrease reflects maturation of a hydrothermal system that is no longer able to effectively scrub magmatic gases (Symonds et al. 2001).

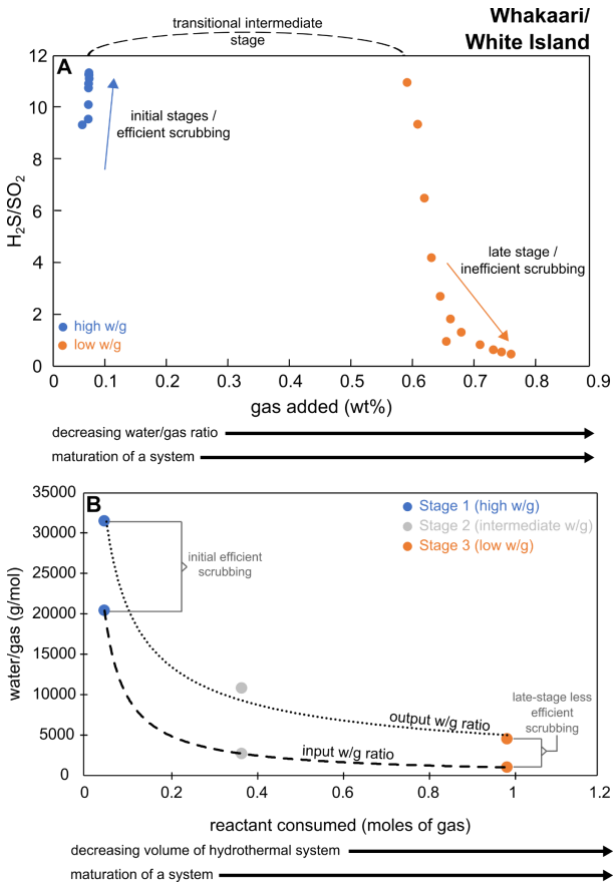

Figure 8 Results from CHIM-XPT modelling of Whakaari: **(a)** changes in H_2S/SO_2 as gas is continually fed into the system. Initially there is a strong scrubbing effect that eventually diminishes as the water/gas ratio decreases; **(b)** displays large initial differences between

compiled input and output gases. Difference between the input and output decreases as gas is added and the system evolves. Dashed line: input gases (before gas-water interaction). Dotted line: output gases after gas-water interaction.

To determine the evolution of gases at Whakaari's hydrothermal system we compare the model input (dashed line) vs. outputs (dotted line) for combined gases (CO_2, H_2O, HCl, SO_2) (Figure 8b). The output compositions and w/g ratios are the output values after the gas-water interaction. We progressively increase input gas contents into the model at three defined stages: (1) high w/g, where a low amount of gas is input through the system, (2) intermediate w/g, where progressively more gas is input, and (3) low w/g, where the highest amount of gas has been titrated through the system comparatively. These three stages represent the progression and evolution of a hydrothermal system as it experiences continual gas input and transitions from an immature (high w/g) to mature (low w/g) hydrothermal system with established gas pathways. We observe a significant change in w/g for the initial stage of high w/g where only a small amount of gas is titrated through the system. The output for this stage shows the w/g increases meaning the initial gas input has been scrubbed and therefore is not degassed out of the hydrothermal water (Figure 8b). It is important to note this change between input and output w/g changes as the system receives more gas going through it. As more gas is incorporated into the system at intermediate w/g and low w/g stages, the output w/g ratio decreases suggesting scrubbing becomes less efficient as a system evolves and more gas is able to pass through without the effect of scrubbing.

On the ternaries in Figure 7a and b, the gas compositions related to the immature stage are shown by the blue polygon and compositions related to the mature stage are the grey polygon. Significant sulfur scrubbing occurs during the immature stage, resulting in a decrease in the CO_2/H_2S ratio as shown by the blue region in Figure 7b. The modeled gas outputs for this immature, high w/g system (blue region) do not overlap with any of the measured fumarole or plume data. For the mature stage (grey region in Figure 7b) we see the effects of scrubbing decrease as the concentration of SO_2 in the gas output increases. The modeled gas outputs with the highest SO_2 concentrations result in the only overlap with measured fumarole and plume compositions. Similar to the EQ3/6 modeled outputs, most of the measured compositions are not recreated by the CHIM-XPT model (Figure 7a and b).

5 Discussion

5.1 The effect of the hydrothermal system on surface gas emissions

To understand the effect of the hydrothermal system on the surface sulfur flux, we compare the gas compositions from our modeling results of magmatic degassing and water-gas-rock reactions to observed fumarole and plume compositions (Figure 7). These represent two end-member scenarios: magmatic degassing (D-Compress and SolEx) models calculate changing gas composition from depth with no interaction with hydrothermal fluids, whereas water-gas-rock reactions (EQ3/6 and CHIM-XPT) force all of the emitted magmatic gas to interact with a hydrothermal fluid. We also compare the pressures derived from the magmatic degassing models that match observed fumarole/plume compositions to the crystallisation modelling using MELTS.

At Whakaari, MELTS modelling suggests crystallisation at 1500 bars, whereas the gas compositions matching observations are produced at 150–650 bars using D-Compress. The difference in depth between MELTS and D-Compress modeling suggests degassing is occurring at shallower depths than crystallisation. A difference in depth between crystallisation

and degassing is not unreasonable given the very simplistic assumption used that the gas separates from the melt at a single pressure, when in reality degassing will occur throughout the magmatic system and gases will mix as they ascend (e.g., Iacovino 2015). The discrepancy in modelled degassing pressure could also result from the solubility constants for a basaltic melt composition in D-Compress poorly representingthe andesitic melt composition of Whakaari. Alternatively, the discrepancy might be an indication that the choice of initial volatile contents used for D-Compress modelling were too low or that open-system degassing is occurring rather than closed-system as modelled here.

Despite these uncertainties, the fumarole and plume compositions at Whakaari are better reproduced by models of magmatic degassing (i.e., D-Compress) than models that force magmatic input gases to interact with hydrothermal fluids (i.e., EQ3/6 or CHIM-XPT) (Figure 7a and b). Fumarole and plume compositions more consistent with models of magmatic degassing are the result of magmatic gases being emitted without large-scale interaction with hydrothermal fluids and can partially be accounted for without any water-gas-rock interactions in the hydrothermal system (unaltered dacite in the case of Whakaari). CHIM-XPT modelled data also shows a trend toward measured fumarole and plume compositions as the system evolves to lower w/g (water/gas) ratio (grey region in Figure 7b). This suggests Whakaari represents a mature hydrothermal system with a low w/g ratio and we refer to this magmatic gas pathway with a low water-gas interaction as a "dry gas pathway". The formation of dry gas pathways is more likely to occur in volcanic systems like Whakaari that have prolonged periods of elevated activity (Symonds et al., 2001). This interpretation is consistent with Christensen et al. (2017), who proposed that large-scale deposition of hydrothermal minerals at Whakaari, such as elemental sulfur and anhydrite, can form a seal which creates a zone where a vapor-dominated phase can exist with low gas-water interaction.

However, some of the low *T* fumaroles are more H_2O-rich than results from magmatic degassing modelling (Figure 7a). Also, the SO_2/H_2S ratio of plume gas is higher than low and high *T* fumaroles (Figure 7b). Magmatic degassing modelling using D-Compress effectively reproduces the plume compositions, but poorly reproduces most of the low and high *T* fumarole compositions, similarly to EQ3/6 and CHIM-XPT (Figure 7b). These compositions could be the result of mixing between magmatic gases (represented by D-Compress results) and magmatic gases that have equilibrated with hydrothermal water (represented by EQ3/6 and CHIM-XPT results). Hence, fumarolic gas compositions from Whakaari likely result from some involvement of the hydrothermal system. For instance, recent electrical resistivity studies of the Whakaari hydrothermal system suggest the presence of a two-phase zone, likely comprised of gases in equilibrium with the hydrothermal system and higher temperature gases in equilibrium with the magma (Miller et al., 2020). Modeled interactions between only magmatic gas and lake water (green triangles in Figure 7a and b) do not produce output gas compositions that overlap with either measured plume or fumarole compositions at Whakaari. However, the presence of the lake likely does play some role in modulating hydrostatic pressure (Christenson et al., 2017), an effect that we have not modeled here.

At Etna, observed melt compositions can be reproduced at a variety of pressures (the best-fit was obtained at 500 bar, but 2000 bar also gave similar results), and the gas composition can be reproduced at a variety of depths, depending on the initial volatile content of the melt. The magmatic plumbing system at Etna is known to be complex, with multiple magma reservoirs present (e.g., Cashman & Edmonds, 2019). Therefore, gases are likely to be mixed from multiple depths to produce the gas composition at the surface.

Our EQ3/6 models produce gas outputs with too low SO_2/H_2S values, whereas SolEx models had SO_2/H_2S within the range of observed emissions (Figure 7d). Overall, gases modeled without hydrothermal interaction (through SolEx) recreated the compositions of

measured gases better than models from EQ3/6. Increasing the SO_2 concentration of our initial magmatic gas to $CO_2/SO_2 = 1$ can result in output gas compositions that better align with measured compositions after interaction with the hydrothermal system: e.g., an initial magmatic gas with $CO_2/SO_2 = 1$ titrated through a brine at high pressure and temperature (300 °C and 50 bars, red X symbols in Figure 7d) results in a SO_2/H_2S ratio that overlaps measured fumarole and plume compositions. However, such a low magmatic CO_2/SO_2 ratio is unlikely. Therefore, our results suggest that shallow scrubbing processes are not occurring on a large-scale at Etna (Figure 7d). This supports Liotta et al. (2010), who found that water-gas interactions at Etna likely occur at pressures between 50–200 bars and temperatures between 270–370°C based on thermochemical modeling (using the software HSC Chemistry) of cooling and condensing magmatic gases under a variety of temperatures and pressures from depth to surface at Etna. At lower temperatures and pressures, the interaction between fluids and ascending magmatic gases is too fast to allow for significant scrubbing of SO_2 at Etna (Giammanco et al., 1998; Liotta et al., 2010). Unfortunately, modeling of our data beyond 300°C was not possible using EQ3/6, limiting our ability to model gas-water interactions at higher temperatures. However, SolEx could not model the full range of measured SO_2/H_2S values of fumarole and plume gases emitted at Etna, suggesting that some extent of hydrothermal interaction must exist to produce lower SO_2/H_2S ratios than what results from magma degassing alone.

5.2 Sulfur inputs and outputs over long time-scales

Our modeling of Whaakari and Etna suggest that over long timescales (decades to 10s kyrs), sulfur inputs from mantle-derived primary magma can balance sulfur outputs as gaseous emissions to the atmosphere, if I:E 1:3 to 1:1 (Whakaari) or 2:1 (Etna) (Figures 2 and 6). If I:E is < 1:3 for Whakaari (which is less than the minimum required to produce the composition of material erupted at the surface), additional sources of sulfur apart from the mantle-derived primary magma would be required (e.g., shallow crustal assimilation). For I:E > 1:1 for Whakaari or 5:1 for Etna, the sulfur output to the atmosphere is less than what is delivered by the long-term average mantle-derived primary magma input, which requires sulfur sequestration. Sulfur sequestration via hydrothermal scrubbing (i.e., gas interactions with water±rock) are found to have limited effect at Whakaari and Etna (see Section 5.1 for full discussion). Therefore, the amount of sulfur sequestered by the hydrothermal systems of these volcanoes must be relatively small or relatively constant over geologic timescales, even though the presence/absence and size of a hydrothermal system can significantly affect the release of sulfur to the atmosphere over short (years to decades) timescales (Giggenbach 1987). However, there are other processes that can sequester sulfur that we did not model, some of which are discussed below.

Magmatic sulfide-saturation is thought to occur in the magmatic systems of both Whakaari and Etna (e.g., Spilliaert et al., 2006; Moretti et al., 2018; Mandon et al., 2020, 2021) – magmatic anhydrite has not been observed at either system. Sulfides are observed in Whakaari magmas as inclusions within minerals, in melt inclusions, and in the groundmass (Mandon et al., 2021). 2–20 t/d of copper is sequestered in the sub-surface, which if caused by late stage sulfide-saturation (~27 wt% Cu and 24–34 wt% S) would result in ~2–20 t/d S also being sequestered (Mandon et al., 2020). Alternatively, these sulfides could be remobilised and broken-down to contribute to degassed S. However, this S flux is smaller than the error in the average S flux between 2005-2015 (71 t/d). Sulfide globules are also observed in melt inclusions and matrix glass from Etna but their occurrence is rare (e.g., Metrich et al., 2004; Spilliaert et al., 2006; Moretti et al. 2018; Gennarro et al. 2019, 2020). Additionally, some of the sulfide globules may have exsolved post-entrapment during cooling in lava flows and

therefore do not necessarily represent primary sulfide-saturation (e.g., 2013 lava flow samples from Gennaro et al., 2019). Primary sulfide-saturation is thought to occur at Etna (e.g., Spilliaert et al., 2006; Moretti et al., 2018). However, sulfide-saturation is only thought to change melt sulfur concentrations temporarily (i.e., sulfides are often resorbed prior to eruption) and at a local spatial scale and therefore does not remove large amounts of sulfur from the system (e.g., Spilliaert et al., 2006; Gennaro et al., 2020). Hence, in both cases, removal of sulfur by magmatic sulfides is not thought to be important.

High-temperature gas-solid reactions can also sequester sulfur in the sub-surface. Henley & Fischer (2021) found the potential for substantial sequestration of SO_2 through reactions with plagioclase and other Ca-bearing minerals, which produces anhydrite and reduced sulfur. Their modelling work showed that in andesitic systems with abundant Ca-bearing minerals this process could remove up to half of the mantle-derived sulfur from the high-temperature gas phase before it reaches the surface and increase fumarole C/S ratios (Henley & Fischer, 2021). If this process is important at Whakaari and/or Etna, it would suggest I:E > 5 for these systems. However, it is unclear for how long the sulfur is removed and how easily it would be remobilised.

At the surface, incomplete degassing of sulfur could also decrease the proportion of mantle-derived sulfur that is degassed at the surface during eruption. However, comparison of sulfur concentrations in whole rock data to initial melt inclusions suggest 92 % of sulfur is degassed at Whakaari during eruption (Mandon et al., 2020).

In summary, mantle-derived sulfur can explain the sulfur emissions from Whakaari and Etna if I:E > 5. If I:E < 5 additional sulfur is required, which is inconsistent with additional constraints on these systems. If I:E > 5, sulfur must be sequestered prior to surface emission: magmatic sulphide formation, hydrothermal scrubbing, and incomplete degassing are unlikely to be important processes for this, but high-temperature gas-solid reactions could be.

5.3 Limitations

Our modelling of the volcanic systems at Whakaari and Etna are only as good as the data and models available. Ample bulk rock data are available for both systems, and the MELTS model is calibrated over a wide compositional range, hence the petrological modelling is likely robust. Although the sulfur content of the mantle feeding both volcanic systems is an important factor, the large uncertainties in the amount of sulfur being released from the slab at either system makes this difficult to constrain. Etna has abundant, Mg-rich olivine-hosted, basaltic melt inclusions, whereas Whakaari erupts predominantly more evolved material, which contains sparse olivine-hosted melt inclusions (e.g., Mandon et al., 2020; Kilgour et al., 2021), implyingthe initial sulfur content of Etna is more reliable than for Whakaari. However, the high S contents recorded in some olivine-hosted melt inclusions at Whakaari suggests these likely represent the initial S content of the primary magma.

A major limitation in our current approach is the suitability of available models for andesite degassing. Firstly, CO_2 solubility is highly melt composition dependent and its partitioning between melt and gas is important for general degassing trends (Brooker et al., 2001; Wallace, 2005; Papale et al., 2006; Moore, 2008). The uncertainty in CO_2 solubility is especially problematic for Whakaari, which has a predominantly andesitic composition, as there is limited experimental data available for similar compositions (e.g., review by Weiser et al., in review) resulting in a lack of andesite solubility constants. Similarly, the default solubility constants in D-Compress for S-bearing species may not be appropriate for andesitic melts. Although andesite-specific solubility constants could be derived from experimental data in the literature and used in D-Compress, this requires knowledge of f_{H2S} and f_{SO2}, which are

not commonly estimated (and insufficient data are typically available to calculate them using thermodynamic equilibria). Also, the initial sulfur content of the melt cannot be independently varied in D-Compress. SolEx, although well-calibrated for Etna, does not model the speciation of sulfur in the gas phase. Hence, it is difficult to directly compare SolEx results to water-gas reaction modelling and plume/fumarole data without subsequent thermodynamic equilibrium calculations to derive H_2S/SO_2 ratios as done here.

Both volcanic systems had sufficient observational data to enable hydrothermal modelling using CHIM-XPT and EQ3/6. However, the current temperature range of these models (maximum 300–400°C) does limit there applicability to certain systems. This is especially true in the case of Etna where high temperature water-gas interactions may play a larger role than what we were able to model (Liotta et al., 2010). Additionally, in EQ3/6 modeling, we do not account for the presence of a separate volatile phase but rather force all high temperature gases at depth through a packet of hydrothermal water. Extending the hydrothermal modelling approach to include high-temperature gas-rock interactions (although the longevity of this interaction is unknown; e.g., Henley & Fischer, 2021) would be a further improvement and constraint on these two volcanic systems. Unfortunately, it would be difficult to extend this modeling attempt to most volcanoes due to insufficient data. However, testing our modeling approach at other well characterised systems (e.g., Ruapehu, Aotearoa New Zealand; Stromboli, Italy; Masaya, Nicaragua; Kīlauea, Hawaii) would help to evaluate the robustness of our generalisations.

6 Conclusions

Overall, we find that long-term inputs of sulfur into the volcanic systems at Whakaari and Etna can be broadly balanced by sulfur outputs over geologic timescales (decades to 10s kyrs). Using thermodynamic, degassing, and hydrothermal models we match measured gas compositions with observational constraints on the magmatic system as model inputs. Small intrusive to extrusive ratios (I:E) would require additional sulfur sources to the mantle, which is inconsistent with other data on these volcanoes. High I:E would require that sulfur is sequestered rather than being degassed to the atmosphere, such as during high-temperature gas-solid reactions (as magmatic sulfide formation, hydrothermal scrubbing, and incomplete degassing are unlikely to be important). However, hydrothermal systems significantly modulate the quantity of emitted sulfur over shorter timescales (years–decades). The extent of scrubbing is dependent on the chemistry and maturity of the hydrothermal system, where there is a strong relationship between scrubbing and the water/gas ratio of the hydrothermal system.

At Whakaari, modeling of magmatic gases emitted through various ground and lake water chemistries results in SO_2/H_2S values that are too low in modeled versus measured gases. The higher SO_2/H_2S values for measured plume and fumarole gases suggests that a portion of magmatic gas is being emitted without interaction with hydrothermal water. Similarly, two end-member scenarios were tested at Etna: forcing all of the magmatic gas to interact with hydrothermal water or having no interaction between gas and water. Measured fumarole and plume data show gases emitted from Etna are not fully described by a low water-gas interaction, suggesting the need for some hydrothermal interaction to fully describe the range of measured gas compositions.

Data availability

All data collated from the literature and used for this study are included in supplementary, as are any results from the modelling described in the paper.

Acknowledgements

This project originated at the Cooperative Institute for Dynamic Earth Research (CIDER) 2019 Summer Program: Volcanoes funded by NSF Grant EAR-1664595 to Bruce Buffett, Barbara Romanowicz, Roland Burgmann, Michael Manga, and Richard Allen. ECH was supported by a Geology Option Post-Doctoral Fellowship from Caltech, CA USA, and the New Zealand Ministry of Business, Innovation and Employment (MBIE) through the Hazards and Risk Management and New Zealand Geothermal Futures programmes (Strategic Science Investment Fund, contract C05X1702). JB was supported by NSF EAR Award #2052963. IMF was supported at UC Berkeley by an NSF Graduate Research Fellowship

References

Aiuppa, A., Federico, C., Giudice, G., Gurrieri, S., Liuzzo, M., Shinohara, H., Favara, R. and Valenza, M., 2006. Rates of carbon dioxide plume degassing from Mount Etna volcano. *Journal of Geophysical Research: Solid Earth*, *111*(B9).

Aiuppa, A., Moretti, R., Federico, C., Giudice, G., Gurrieri, S., Liuzzo, M., Papale, P., Shinohara, H. and Valenza, M., 2007. Forecasting Etna eruptions by real-time observation of volcanic gas composition. *Geology*, *35*(12), pp.1115-1118.

Aiuppa, A., Giudice, G., Gurrieri, S., Liuzzo, M., Burton, M., Caltabiano, T., McGonigle, A.J.S., Salerno, G., Shinohara, H. and Valenza, M., 2008. Total volatile flux from Mount Etna. *Geophysical Research Letters*, *35*(24).

Aiuppa, A., Fischer, T.P., Plank, T., Robidoux, P. and Di Napoli, R., 2017. Along-arc, inter-arc and arc-to-arc variations in volcanic gas CO_2/S_T ratios reveal dual source of carbon in arc volcanism. *Earth-Science Reviews*, *168*, pp.24-47.

Aiuppa, A., Fischer, T.P., Plank, T. and Bani, P., 2019. CO_2 flux emissions from the Earth's most actively degassing volcanoes, 2005–2015. *Scientific reports*, *9*(1), pp.1-17.

Allard, P., Carbonnelle, J., Dajlevic, D., Le Bronec, J., Morel, P., Robe, M.C., Maurenas, J.M., Faivre-Pierret, R., Martin, D., Sabroux, J.C. and Zettwoog, P., 1991. Eruptive and diffuse emissions of CO_2 from Mount Etna. *Nature*, *351*(6325), pp.387-391.

Allard, P., Behncke, B., D'Amico, S., Neri, M. and Gambino, S., 2006. Mount Etna 1993–2005: Anatomy of an evolving eruptive cycle. *Earth-Science Reviews*, *78*(1-2), pp.85-114.

Alt, J. C., Shanks III, W. C., & Jackson, M. C. (1993). Cycling of sulfur in subduction zones: The geochemistry of sulfur in the Mariana Island Arc and back-arc trough. *Earth and Planetary Science Letters*, *119*(4), 477-494.

Alt, J.C., 1995. Sulfur isotopic profile through the oceanic crust: Sulfur mobility and seawater-crustal sulfur exchange during hydrothermal alteration. *Geology*, *23*(7), pp.585-588.

Armienti, P., Innocenti, F., Petrini, R., Pompilio, M., and Villari, L., 1989, Petrology and Sr-Nd isotope geochemistry of recent lavas from Mt. Etna: bearing on the volcano feeding system: Journal of Volcanology and Geothermal Research, v. 39, p. 315–327, doi:10.1016/0377-0273(89)90095-4.

Asimow, P.D. and Ghiorso, M.S., 1998. Algorithmic modifications extending MELTS to calculate subsolidus phase relations. *American mineralogist*, *83*(9-10), pp.1127-1132.

Baker, D.R. and Moretti, R., 2011. Modeling the solubility of sulfur in magmas: a 50-year old geochemical challenge. *Reviews in Mineralogy and Geochemistry*, *73*(1), pp.167-213.

Barberi, F., Civetta, L., Gasparini, P., Innocenti, F., Scandone, R. and Villari, L., 1974. Evolution of a section of the Africa-Europe plate boundary: paleomagnetic and volcanological evidence from Sicily. *Earth and Planetary Science Letters*, *22*(2), pp.123-132.

Beaudry, P., Longpré, M. A., Economos, R., Wing, B. A., Bui, T. H., & Stix, J. (2018). Degassing-induced fractionation of multiple sulphur isotopes unveils post-Archaean recycled oceanic crust signal in hotspot lava. *Nature communications*, *9*(1), 1-12.

Behncke, B., Calvari, S., Giammanco, S., Neri, M. and Pinkerton, H., 2008. Pyroclastic density currents resulting from the interaction of basaltic magma with hydrothermally altered rock: an example from the 2006 summit eruptions of Mount Etna, Italy. *Bulletin of Volcanology*, *70*(10), pp.1249-1268.

Berner, E.K. and Berner, R.A., 2012. *Global environment: water, air, and geochemical cycles*. Princeton University Press.

Blank, J.G., Stolper, E.M. and Carroll, M.R., 1993. Solubilities of carbon dioxide and water in rhyolitic melt at 850 C and 750 bars. *Earth and Planetary Science Letters*, *119*(1-2), pp.27-36.

Brooker, R.A., Kohn, S.C., Holloway, J.R. and McMillan, P.F., 2001. Structural controls on the solubility of CO2 in silicate melts: part I: bulk solubility data. *Chemical Geology*, *174*(1-3), pp.225-239.

Bruno, N., Caltabiano, T. and Romano, R., 1999. SO2 emissions at Mt. Etna with particular reference to the period 1993–1995. *Bulletin of Volcanology*, *60*(6), pp.405-411.

Brusca, L., Aiuppa, A., D'Alessandro, W., Parello, F., Allard, P. and Michel, A., 2001. Geochemical mapping of magmatic gas–water–rock interactions in the aquifer of Mount Etna volcano. *Journal of Volcanology and Geothermal Research*, *108*(1-4), pp.199-218.

Burgisser, A., Alletti, M. and Scaillet, B., 2015. Simulating the behavior of volatiles belonging to the C–O–H–S system in silicate melts under magmatic conditions with the software D-Compress. *Computers & Geosciences*, *79*, pp.1-14.

Burton, M.R., Neri, M., Andronico, D., Branca, S., Caltabiano, T., Calvari, S., Corsaro, R.A., Del Carlo, P., Lanzafame, G., Lodato, L. and Miraglia, L., 2005. Etna 2004–2005: An archetype for geodynamically-controlled effusive eruptions. *Geophysical research letters*, *32*(9).

Caltabiano, T., Romano, R. and Budetta, G., 1994. SO2 flux measurements at Mount Etna (Sicily). *Journal of Geophysical Research: Atmospheres*, *99*(D6), pp.12809-12819.

Cannata, A., Di Grazia, G., Giuffrida, M., Gresta, S., Palano, M., Sciotto, M., Viccaro, M. and Zuccarello, F., 2018. Space-time evolution of magma storage and transfer at Mt. Etna Volcano (Italy): the 2015–2016 Reawakening of Voragine Crater. *Geochemistry, Geophysics, Geosystems*, *19*(2), pp.471-495.

Carn, S.A., Fioletov, V.E., McLinden, C.A., Li, C. and Krotkov, N.A., 2017. A decade of global volcanic SO 2 emissions measured from space. *Scientific reports*, *7*(1), pp.1-12.

Cashman, K.V. and Edmonds, M., 2019. Mafic glass compositions: a record of magma storage conditions, mixing and ascent. *Philosophical Transactions of the Royal Society A, 377(2139)*.

Chowdhury, P. and Dasgupta, R., 2019. Effect of sulfate on the basaltic liquidus and sulfur Concentration at Anhydrite Saturation (SCAS) of hydrous basalts–Implications for sulfur cycle in subduction zones. *Chemical Geology*, *522*, pp.162-174.

Christenson, B.W., White, S., Britten, K. and Scott, B.J., 2017. Hydrological evolution and chemical structure of a hyper-acidic spring-lake system on Whakaari/White Island, NZ. *Journal of Volcanology and Geothermal Research*, *346*, pp.180-211.

Cicconi, M.R., Le Losq, C., Moretti, R. and Neuville, D.R., 2020. Magmas are the largest repositories and carriers of earth's redox processes. *Elements: An International Magazine of Mineralogy, Geochemistry, and Petrology*, *16*(3), pp.173-178.

Clemente, B., Scaillet, B., and Pichavant, M., 2004. The solubility of sulphur in hydrous rhyolitic melts. *Journal of Petrology* 45(11), pp.2171-2196.

Cole, J.W., 1990. Structural control and origin of volcanism in the Taupo volcanic zone, New Zealand. *Bulletin of volcanology*, *52*(6), pp.445-459.

Cole, J.W., Thordarson, T. and Burt, R.M., 2000. Magma origin and evolution of White Island (Whakaari) volcano, Bay of plenty, New Zealand. *Journal of Petrology*, *41*(6), pp.867-895.

Collins, S. J., Pyle, D. M., & Maclennan, J. (2009). Melt inclusions track pre-eruption storage and dehydration of magmas at Etna. *Geology*, *37*(6), 571-574.

Coltelli, M., Del Carlo, P. and Vezzoli, L., 1998. Discovery of a Plinian basaltic eruption of Roman age at Etna volcano, Italy. *Geology*, *26*(12), pp.1095-1098.

Correale, A., Paonita, A., Martelli, M., Rizzo, A., Rotolo, S.G., Corsaro, R.A., and Di Renzo, V., 2014, A two-component mantle source feeding Mt. Etna magmatism: Insights from the geochemistry of primitive magmas: Lithos, v. 184–187, p. 243–258, doi:10.1016/j.lithos.2013.10.038.

Corsaro, R.A., Miraglia, L., and Pompilio, M., 2007, Petrologic evidence of a complex plumbing system feeding the July–August 2001 eruption of Mt. Etna, Sicily, Italy: Bulletin of Volcanology, v. 69, p. 401–421, doi:10.1007/s00445-006-0083-4.

De Hoog, J.C.M., Taylor, B.E. and Van Bergen, M.J., 2001. Sulfur isotope systematics of basaltic lavas from Indonesia: implications for the sulfur cycle in subduction zones. *Earth and Planetary Science Letters*, *189*(3-4), pp.237-252.

de Moor, J.M., Fischer, T.P., Sharp, Z.D., King, P.L., Wilke, M., Botcharnikov, R.E., Cottrell, E., Zelenski, M., Marty, B., Klimm, K. and Rivard, C., 2013. Sulfur degassing at Erta Ale (Ethiopia) and Masaya (Nicaragua) volcanoes: Implications for degassing processes and oxygen fugacities of basaltic systems. *Geochemistry, Geophysics, Geosystems*, *14*(10), pp.4076-4108.

de Moor, J.M., Aiuppa, A., Avard, G., Wehrmann, H., Dunbar, N., Muller, C., Tamburello, G., Giudice, G., Liuzzo, M., Moretti, R. and Conde, V., 2016a. Turmoil at Turrialba Volcano (Costa Rica): Degassing and eruptive processes inferred from high-frequency gas monitoring. *Journal of Geophysical Research: Solid Earth*, *121*(8), pp.5761-5775.

de Moor, J.M., Aiuppa, A., Pacheco, J., Avard, G., Kern, C., Liuzzo, M., Martinez, M., Giudice, G. and Fischer, T.P., 2016b. Short-period volcanic gas precursors to phreatic eruptions: Insights from Poás Volcano, Costa Rica. *Earth and Planetary Science Letters*, *442*, pp.218-227.

de Moor, J.M., Stix, J., Avard, G., Muller, C., Corrales, E., Diaz, J.A., Alan, A., Brenes, J., Pacheco, J., Aiuppa, A. and Fischer, T.P., 2019. Insights on hydrothermal-magmatic interactions and eruptive processes at Poás Volcano (Costa Rica) from high-frequency gas monitoring and drone measurements. *Geophysical Research Letters*, *46*(3), pp.1293-1302.

Di Napoli, R., Aiuppa, A., Bergsson, B., Ilyinskaya, E., Pfeffer, M.A., Guðjónsdóttir, S.R. and Valenza, M., 2016. Reaction path models of magmatic gas scrubbing. *Chemical Geology*, *420*, pp.251-269.

Di Renzo, V., Corsaro, R.A., Miraglia, L., Pompilio, M., and Civetta, L., 2019, Long and short-term magma differentiation at Mt. Etna as revealed by Sr-Nd isotopes and geochemical data: Earth-Science Reviews, v. 190, p. 112–130, doi:10.1016/j.earscirev.2018.12.008.

Ding, S. and Dasgupta, R., 2018. Sulfur inventory of ocean island basalt source regions constrained by modeling the fate of sulfide during decompression melting of a heterogeneous mantle. *Journal of Petrology*, *59*(7), pp.1281-1308.

Duncan, A.R. and Vucetich, C.G., 1970. Volcanic activity on White Island, bay of plenty, 1966–69: Part 2—tephra eruptions—stratigraphy and petrography. *New Zealand journal of geology and geophysics*, *13*(4), pp.969-979.

Edner, H., Ragnarson, P., Svanberg, S., Wallinder, E., Ferrara, R., Cioni, R., Raco, B. and Taddeucci, G., 1994. Total fluxes of sulfur dioxide from the Italian volcanoes Etna, Stromboli, and Vulcano measured by differential absorption lidar and passive differential optical absorption spectroscopy. *Journal of Geophysical Research: Atmospheres*, *99*(D9), pp.18827-18838.

Edwards, M.J. and Pioli, L., 2019. Magma and tephra characteristics for the 17–25 May 2016 Mt Etna eruption. Data in brief 22, 65-71.

Esposito, R., Hunter, J., Schiffbauer, J.D., Shimizu, N. and Bodnar, R.J., 2014. An assessment of the reliability of melt inclusions as recorders of the pre-eruptive volatile content of magmas. *American Mineralogist*, *99*(5-6), pp.976-998.

Fischer, T.P., Ramírez, C., Mora-Amador, R.A., Hilton, D.R., Barnes, J.D., Sharp, Z.D., Le Brun, M., de Moor, J.M., Barry, P.H., Füri, E. and Shaw, A.M., 2015. Temporal variations in fumarole gas chemistry at Poás volcano, Costa Rica. *Journal of Volcanology and Geothermal Research*, *294*, pp.56-70.

Fischer, T.P., Arellano, S., Carn, S., Aiuppa, A., Galle, B., Allard, P., Lopez, T., Shinohara, H., Kelly, P., Werner, C. and Cardellini, C., 2019. The emissions of CO 2 and other volatiles from the world's subaerial volcanoes. *Scientific reports*, *9*(1), pp.1-11.

Gaborieau, M., Laubier, M., Bolfan-Casanova, N., McCammon, C.A., Vantelon, D., Chumakov, A.I., Schiavi, F., Neuville, D.R. and Venugopal, S., 2020. Determination of Fe3+/ΣFe of olivine-hosted melt inclusions using Mössbauer and XANES spectroscopy. *Chemical Geology*, *547*, p.119646.

Gennaro, E., Iacono-Marziano, G., Paonita, A., Rotolo, S.G., Martel, C., Rizzo, A.L., Pichavant, M. and Liotta, M., 2019. Melt inclusions track melt evolution and degassing of Etnean magmas in the last 15 ka. *Lithos*, *324*, pp.716-732.

Gennaro, E., Paonita, A., Iacono-Marziano, G., Moussallam, Y., Pichavant, M., Peters, N. and Martel, C., 2020. Sulphur behaviour and redox conditions in etnean magmas during magma differentiation and degassing. *Journal of Petrology*.

Ghiorso, M.S. and Sack, R.O., 1995. Chemical mass transfer in magmatic processes IV. A revised and internally consistent thermodynamic model for the interpolation and extrapolation of liquid-solid equilibria in magmatic systems at elevated temperatures and pressures. *Contributions to Mineralogy and Petrology*, *119*(2), pp.197-212.

Ghiorso, M.S., Hirschmann, M.M., Reiners, P.W. and Kress, V.C., 2002. The pMELTS: A revision of MELTS for improved calculation of phase relations and major element partitioning

related to partial melting of the mantle to 3 GPa. *Geochemistry, Geophysics, Geosystems, 3(5)*, pp.1-35.

Giammanco, S., Inguaggiato, S. and Valenza, M., 1998. Soil and fumarole gases of Mount Etna: geochemistry and relations with volcanic activity. *Journal of volcanology and geothermal research*, *81*(3-4), pp.297-310.

Giggenbach, W.F., 1975. Variations in the carbon, sulfur and chlorine contents of volcanic gas discharges from White Island, New Zealand. *Bulletin Volcanologique*, *39*(1), pp.15-27.

Giggenbach, W., 1982. The chemical and isotopic composition of gas discharges from New Zealand andesitic volcanoes. *Bulletin volcanologique*, *45*(3), pp.253-255.

Giggenbach, W.F., 1987. Redox processes governing the chemistry of fumarolic gas discharges from White Island, New Zealand. *Applied Geochemistry*, *2*(2), pp.143-161.

Giggenbach, W.F., Shinohara, H., Kusakabe, M. and Ohba, T., 2003. Formation of acid volcanic brines through interaction of magmatic gases, seawater, and rock within the White Island volcanic-hydrothermal system, New Zealand. *Special Publication-Society of Economic Geologists*, *10*, pp.19-40.

Giuffrida, M. and Viccaro, M., 2017. Three years (2011–2013) of eruptive activity at Mt. Etna: working modes and timescales of the modern volcano plumbing system from micro-analytical studies of crystals. *Earth-Science Reviews*, *171*, pp.289-322.

Goff, F., Janik, C.J., Delgado, H., Werner, C., Counce, D., Stimac, J.A., Siebe, C., Love, S.P., Williams, S.N., Fischer, T. and Johnson, L., 1998. Geochemical surveillance of magmatic volatiles at Popocatépetl volcano, Mexico. *Geological Society of America Bulletin*, *110*(6), pp.695-710.

Goff, F., Love, S.P., Warren, R.G., Counce, D., Obenholzner, J., Siebe, C. and Schmidt, S.C., 2001. Passive infrared remote sensing evidence for large, intermittent CO2 emissions at Popocatépetl volcano, Mexico. *Chemical Geology*, *177*(1-2), pp.133-156.

Goff, F. and McMurtry, G.M., 2000. Tritium and stable isotopes of magmatic waters. *Journal of Volcanology and Geothermal Research*, *97*(1-4), pp.347-396.

Hao, J., Sverjensky, D.A. and Hazen, R.M., 2017. A model for late Archean chemical weathering and world average river water. *Earth and Planetary Science Letters*, *457*, pp.191-203.

Harris, A., Steffke, A., Calvari, S. and Spampinato, L., 2011. Thirty years of satellite-derived lava discharge rates at Etna: Implications for steady volumetric output. *Journal of Geophysical Research: Solid Earth*, *116*(B8).

Heap, M.J., Kennedy, B.M., Farquharson, J.I., Ashworth, J., Mayer, K., Letham-Brake, M., Reuschle, T., Gilg, H.A., Scheu, B., Lavallee, Y. and Siratovich, P., 2017. A multidisciplinary approach to quantify the permeability of the Whakaari/White Island volcanic hydrothermal system (Taupo Volcanic Zone, New Zealand). *Journal of Volcanology and Geothermal Research*, *332*, pp.88-108.

Henley, R.W. and Fischer, T.P., 2021. Sulfur sequestration and redox equilibria in volcanic gases. *Journal of Volcanology and Geothermal Research*, *414*, p.107181.

Heyworth, Z., Turner, S., Schaefer, B., Wood, B., George, R., Berlo, K., Cunningham, H., Price, R., Cook, C., and Gamble, J., 2007, 238U–230Th–226Ra–210Pb constraints on the genesis of high-Mg andesites at White Island, New Zealand: Chemical Geology, v. 243, p. 105–121, doi:10.1016/j.chemgeo.2007.05.012.

Holland, T., and Roger, P., 1991. "A compensated-Redlich-Kwong (CORK) equation for volumes and fugacities of CO_2 and H_2O in the range 1 bar to 50 kbar and 100–1600 °C." *Contributions to Mineralogy and Petrology, 109*(2), pp.265-273.

Hutchison, W., Finch, A.A. and Boyce, A.J., 2020. The sulfur isotope evolution of magmatic-hydrothermal fluids: insights into ore-forming processes. *Geochimica et Cosmochimica Acta*, *288*, pp.176-198.

Jolly, A.D., Lokmer, I., Thun, J., Salichon, J., Fry, B. and Chardot, L., 2017. Insights into fluid transport mechanisms at White Island from analysis of coupled very long-period (VLP), long-period (LP) and high-frequency (HF) earthquakes. *Journal of Volcanology and Geothermal Research*, *343*, pp.75-94.

Kamenetsky, V.S., Pompilio, M., Métrich, N., Sobolev, A.V., Kuzmin, D.V., and Thomas, R., 2007, Arrival of extremely volatile-rich high-Mg magmas changes explosivity of Mount Etna: Geology, v. 35, p. 255–258, doi:10.1130/G23163A.1.

Kagoshima, T., Sano, Y., Takahata, N., Maruoka, T., Fischer, T.P. and Hattori, K., 2015. Sulphur geodynamic cycle. *Scientific Reports*, *5*(1), pp.1-6.

Kilgour, G., Kennedy, B., Scott, B., Christenson, B., Jolly, A., Asher, A., Rosenberg, M. and Saunders, K., 2021. Whakaari/White Island: a review of New Zealand's most active volcano. *New Zealand Journal of Geology and Geophysics*, *64*.

Kilgour GN, Moune S, Christenson BW, Della Pasqua F., 2021. Insights into the 1976–2000 eruption episode of Whakaari/White Island, New Zealand: an eruption fuelled by repeated mafic recharge. *Bulletin of Volcanology, 83.*

La Spina, A., Burton, M. and Salerno, G.G., 2010. Unravelling the processes controlling gas emissions from the central and northeast craters of Mt. Etna. *Journal of Volcanology and Geothermal Research*, 198(3-4), pp.368-376.

Labidi, J., Cartigny, P., Birck, J.L., Assayag, N. and Bourrand, J.J., 2012. Determination of multiple sulfur isotopes in glasses: A reappraisal of the MORB δ34S. *Chemical Geology*, *334*, pp.189-198.

Labidi, J., & Cartigny, P. (2016). Negligible sulfur isotope fractionation during partial melting: Evidence from Garrett transform fault basalts, implications for the late-veneer and the hadean matte. *Earth and Planetary Science Letters*, *451*, 196-207.

Lee, C.T.A., Erdman, M., Yang, W., Ingram, L., Chin, E.J. and DePaolo, D.J., 2018. Sulfur isotopic compositions of deep arc cumulates. *Earth and Planetary Science Letters*, *500*, pp.76-85.

Li, J.L., Schwarzenbach, E.M., John, T., Ague, J.J., Huang, F., Gao, J., Klemd, R., Whitehouse, M.J. and Wang, X.S., 2020. Uncovering and quantifying the subduction zone sulfur cycle from the slab perspective. *Nature communications*, *11*(1), pp.1-12.

Liotta, M., Paonita, A., Caracausi, A., Martelli, M., Rizzo, A. and Favara, R., 2010. Hydrothermal processes governing the geochemistry of the crater fumaroles at Mount Etna volcano (Italy). *Chemical Geology*, *278*(1-2), pp.92-104.

Liotta, M., Rizzo, A., Paonita, A., Caracausi, A. and Martelli, M., 2012. Sulfur isotopic compositions of fumarolic and plume gases at Mount Etna (Italy) and inferences on their magmatic source. *Geochemistry, Geophysics, Geosystems*, *13*(5).

Lopez, T., Aguilera, F., Tassi, F., De Moor, J.M., Bobrowski, N., Aiuppa, A., Tamburello, G., Rizzo, A.L., Liuzzo, M., Viveiros, F. and Cardellini, C., 2018. New insights into the magmatic-

hydrothermal system and volatile budget of Lastarria volcano, Chile: Integrated results from the 2014 IAVCEI CCVG 12th Volcanic Gas Workshop. *Geosphere*, *14*(3), pp.983-1007.

Mandeville, C.W., Sasaki, A., Saito, G., Faure, K., King, R. and Hauri, E., 1998. Open-system degassing of sulfur from Krakatau 1883 magma. *Earth and Planetary Science Letters*, *160*(3-4), pp.709-722.

Mandeville, C.W., Webster, J.D., Tappen, C., Taylor, B.E., Timbal, A., Sasaki, A., Hauri, E. and Bacon, C.R., 2009. Stable isotope and petrologic evidence for open-system degassing during the climactic and pre-climactic eruptions of Mt. Mazama, Crater Lake, Oregon. *Geochimica et Cosmochimica Acta*, *73*(10), pp.2978-3012.

Mandon, C.L., Seward, T.M. and Christenson, B.W., 2020. Volatile transport of metals and the Cu budget of the active White Island magmatic-hydrothermal system, New Zealand. *Journal of Volcanology and Geothermal Research*, *398*, p.106905.

Mandon, C.L., Christenson, B.W., Seward T.M., Schipper, C.I., 2021. Magma mixing, degassing and late sulfide saturation: Insights into the 1976–2000 eruptive sequence at White Island, New Zealand. Journal of Volcanology and Geothermal Research,

Marini, L., Moretti, R. and Accornero, M., 2011. Sulfur isotopes in magmatic-hydrothermal systems, melts, and magmas. *Reviews in Mineralogy and Geochemistry*, *73*(1), pp.423-492.

McCollom, T.M., 2007. Geochemical constraints on sources of metabolic energy for chemolithoautotrophy in ultramafic-hosted deep-sea hydrothermal systems. *Astrobiology*, *7*(6), pp.933-950.

Métrich, N., Allard, P., Spilliaert, N., Andronico, D. and Burton, M., 2004. 2001 flank eruption of the alkali-and volatile-rich primitive basalt responsible for Mount Etna's evolution in the last three decades. *Earth and Planetary Science Letters*, *228*(1-2), pp.1-17.

Miller, C.A., Christenson, B.W., Byrdina, S., Vandemeulebrouck, J., Brakenrig, T., Britten, K., Shanks, J. and Epstein, G., 2020. Snapshot of a magmatic/hydrothermal system from electrical resistivity tomography and fumarolic composition, Whakaari/White Island, New Zealand. *Journal of Volcanology and Geothermal Research*, *400*, p.106909.

Moore, G., 2008. Interpreting H2O and CO2 contents in melt inclusions: constraints from solubility experiments and modeling. *Reviews in Mineralogy and Geochemistry*, *69*(1), pp.333-362.

Moore, L.R., Gazel, E., Tuohy, R., Lloyd, A.S., Esposito, R., Steele-MacInnis, M., Hauri, E.H., Wallace, P.J., Plank, T. and Bodnar, R.J., 2015. Bubbles matter: An assessment of the contribution of vapor bubbles to melt inclusion volatile budgets. *American Mineralogist*, *100*(4), pp.806-823.

Moretti, R., Métrich, N., Arienzo, I., Di Renzo, V., Aiuppa, A. and Allard, P., 2018. Degassing vs. eruptive styles at Mt. Etna volcano (Sicily, Italy). Part I: Volatile stocking, gas fluxing, and the shift from low-energy to highly explosive basaltic eruptions. *Chemical Geology*, *482*, pp.1-17.

Moretti, R. and Stefánsson, A., 2020. Volcanic and geothermal redox engines. *Elements: An International Magazine of Mineralogy, Geochemistry, and Petrology*, *16*(3), pp.179-184.

Ohmoto, H., 1972. Systematics of sulfur and carbon isotopes in hydrothermal ore deposits. *Economic Geology*, *67*(5), pp.551-578.

Ohmoto, H. and Kerrick, D.M., 1977. Devolatilization equilibria in graphitic systems. American Journal of Science, 277(8), pp.1013-1044.

Papale, P., Moretti, R. and Barbato, D., 2006. The compositional dependence of the saturation surface of H2O+ CO2 fluids in silicate melts. *Chemical Geology*, *229*(1-3), pp.78-95.

Patanè, D., Aiuppa, A., Aloisi, M., Behncke, B., Cannata, A., Coltelli, M., Di Grazia, G., Gambino, S., Gurrieri, S., Mattia, M. and Salerno, G., 2013. Insights into magma and fluid transfer at Mount Etna by a multiparametric approach: A model of the events leading to the 2011 eruptive cycle. *Journal of Geophysical Research: Solid Earth*, *118*(7), pp.3519-3539.

Potter, N.J., Carey, R.J., Andronico, D. and Costantini, L., 2019. Eruption dynamics of the 23 February 2013 event at Mt. Etna. Journal of Volcanology and Geothermal Research, 384, pp.241-250.

Pugnaghi, S., Gangale, G., Corradini, S. and Buongiorno, M.F., 2006. Mt. Etna sulfur dioxide flux monitoring using ASTER-TIR data and atmospheric observations. Journal of Volcanology and Geothermal Research, 152(1-2), pp.74-90.

Rapien, M.H., Bodnar, R.J., Simmons, S.F., Szabo, C.S., Wood, C.P. and Sutton, S.R., 2003. Melt inclusion study of the embryonic porphyry copper system at White Island, New Zealand. *Special Publication-Society of Economic Geologists*, *10*, pp.41-60.

Reed, M.H., Spycher, N.F. and Palandri, J., 2016. Users Guide for CHIM-XPT: A Program for Computing Reaction Processes in Aqueous-Mineral-Gas Systems and MINTAB Guide, Version 2.50. *Eugene, OR: University of Oregon*.

Richet, P., Bottinga, Y. and Javoy, M., 1977. A review of hydrogen, carbon, nitrogen, oxygen, sulphur, and chlorine stable isotope fractionation among gaseous molecules. *Annual Review of Earth and Planetary Sciences*, *5*(1), pp.65-110.

Robinson, B.W., 1987. Sulphur and sulphate-oxygen isotopes in New Zealand geothermal systems and volcanic discharges. In *Studies on sulphur isotope variations in nature*.

Salerno, G.G., Burton, M.R., Oppenheimer, C., Caltabiano, T., Randazzo, D., Bruno, N. and Longo, V., 2009. Three-years of SO2 flux measurements of Mt. Etna using an automated UV scanner array: Comparison with conventional traverses and uncertainties in flux retrieval. *Journal of Volcanology and Geothermal Research*, *183*(1-2), pp.76-83.

Schiano, P., Clocchiatti, R., Ottolini, L. and Busa, T., 2001. Transition of Mount Etna lavas from a mantle-plume to an island-arc magmatic source. *Nature*, *412*(6850), pp.900-904.

Schiavi, F., Rosciglione, A., Kitagawa, H., Kobayashi, K., Nakamura, E., Nuccio, P.M., Ottolini, L., Paonita, A. and Vannucci, R., 2015. Geochemical heterogeneities in magma beneath Mount Etna recorded by 2001–2006 melt inclusions. *Geochemistry, Geophysics, Geosystems*, *16*(7), pp.2109-2126.

Shane, P., Sikes, E.L. and Guilderson, T.P., 2006. Tephra beds in deep-sea cores off northern New Zealand: implications for the history of Taupo Volcanic Zone, Mayor Island and White Island volcanoes. *Journal of Volcanology and Geothermal Research*, *154*(3-4), pp.276-290.

Shaw, H.R., 1985. Links between magma-tectonic rate balances, plutonism, and volcanism. *Journal of Geophysical Research: Solid Earth*, *90*(B13), pp.11275-11288.

Shi, P. and Saxena, S.K., 1992. Thermodynamic modelling of the CHOS fluid system. *American Mineralogist*, *77*(9-10), pp.1038-1049.

Shinohara, H., Aiuppa, A., Giudice, G., Gurrieri, S. and Liuzzo, M., 2008. Variation of H2O/CO2 and CO2/SO2 ratios of volcanic gases discharged by continuous degassing of Mount Etna volcano, Italy. *Journal of Geophysical Research: Solid Earth*, *113*(B9).

Spilliaert, N., Allard, P., Métrich, N. and Sobolev, A.V., 2006. Melt inclusion record of the conditions of ascent, degassing, and extrusion of volatile-rich alkali basalt during the powerful

2002 flank eruption of Mount Etna (Italy). *Journal of Geophysical Research: Solid Earth*, *111*(B4).

Steffke, A.M., Harris, A.J.L., Burton, M., Caltabiano, T., Salerno, G.G., 2011. Coupled use of COSPEC and satellite measurements to define the volumetric balance during effusive eruptions at Mt. Etna, Italy. *Journal of Volcanology and Geothermal Research*, 205(1–2):47-53.

Symonds, R.B., Gerlach, T.M. and Reed, M.H., 2001. Magmatic gas scrubbing: implications for volcano monitoring. *Journal of Volcanology and Geothermal Research*, *108*(1-4), pp.303-341.

Tanguy, J.C., Condomines, M. and Kieffer, G., 1997. Evolution of the Mount Etna magma: constraints on the present feeding system and eruptive mechanism. *Journal of Volcanology and Geothermal research*, *75*(3-4), pp.221-250.

Tonarini, S., Armienti, P., D'Orazio, M., Innocenti, F., Pompilio, M., and Petrini, R., 1995, Geochemical and isotopic monitoring of Mt. Etna 1989–1993 eruptive activity: bearing on the shallow feeding system: Journal of Volcanology and Geothermal Research, v. 64, p. 95–115, doi:10.1016/0377-0273(94)00039-J.

Venugopal, S., Schiavi, F., Moune, S., Bolfan-Casanova, N., Druitt, T. and Williams-Jones, G., 2020. Melt inclusion vapour bubbles: the hidden reservoir for major and volatile elements. *Scientific reports*, *10*(1), pp.1-14.

Viccaro, M., Calcagno, R., Garozzo, I., Giuffrida, M., and Nicotra, E., 2015, Continuous magma recharge at Mt. Etna during the 2011–2013 period controls the style of volcanic activity and compositions of erupted lavas: Mineralogy and Petrology, v. 109, p. 67–83, doi:10.1007/s00710-014-0352-4.

Viccaro, M., and Cristofolini, R., 2008, Nature of mantle heterogeneity and its role in the short-term geochemical and volcanological evolution of Mt. Etna (Italy): Lithos, v. 105, p. 272–288, doi:10.1016/j.lithos.2008.05.001.

Wallace, L.M., Beavan, J., McCaffrey, R. and Darby, D., 2004. Subduction zone coupling and tectonic block rotations in the North Island, New Zealand. *Journal of Geophysical Research: Solid Earth*, *109*(B12).

Wallace, P.J., 2003. From mantle to atmosphere: magma degassing, explosive eruptions, and volcanic volatile budgets. In *Developments in volcanology* (Vol. 5, pp. 105-127). Elsevier.

Wallace, P.J., 2005. Volatiles in subduction zone magmas: concentrations and fluxes based on melt inclusion and volcanic gas data. *Journal of volcanology and Geothermal Research*, *140*(1-3), pp.217-240.

Wallace, P.J. and Edmonds, M., 2011. The sulfur budget in magmas: evidence from melt inclusions, submarine glasses, and volcanic gas emissions. *Reviews in Mineralogy and Geochemistry*, *73*(1), pp.215-246.

Wallace, P.J., Kamenetsky, V.S. and Cervantes, P., 2015. Melt inclusion CO2 contents, pressures of olivine crystallization, and the problem of shrinkage bubbles. *American Mineralogist*, *100*(4), pp.787-794.

Wardell, L.J., Kyle, P.R., Dunbar, N. and Christenson, B., 2001. White Island volcano, New Zealand: carbon dioxide and sulfur dioxide emission rates and melt inclusion studies. *Chemical Geology*, *177*(1-2), pp.187-200.

Wieser, P.E., Iacovino, K., Matthews, S, Moore, G.M., and Allison, C. (in review). VESIcal Part II: A critical approach to volatile solubility modelling using an open-source Python3 engine. *Earth and Space Sciences.*

Werner, C.A., Doukas, M.P. and Kelly, P.J., 2011. Gas emissions from failed and actual eruptions from Cook Inlet Volcanoes, Alaska, 1989–2006. *Bulletin of Volcanology*, *73*(2), pp.155-173.

Williams, S.N., Schaefer, S.J., Calvache, V.M.L. and Lopez, D., 1992. Global carbon dioxide emission to the atmosphere by volcanoes. *Geochimica et Cosmochimica Acta*, *56*(4), pp.1765-1770.

Witham, F., Blundy, J., Kohn, S.C., Lesne, P., Dixon, J., Churakov, S.V. and Botcharnikov, R., 2012. SolEx: A model for mixed COHSCl-volatile solubilities and exsolved gas compositions in basalt. *Computers & Geosciences*, *45*, pp.87-97.

Wolery, T J. EQ3/6, a software package for geochemical modeling of aqueous systems: Package overview and installation guide (Version 7.0). United States: N. p., 1992. Web. doi:10.2172/138894.

Wolery, T.J. and Daveler, S.A., 1992. *EQ6, a computer program for reaction path modeling of aqueous geochemical systems: Theoretical manual, users guide, and related documentation (Version 7.0); Part 4* (No. UCRL-MA-110662-Pt. 4). Lawrence Livermore National Lab., CA (United States).

Zheng, Y.F. and Hoefs, J., 1993. Effects of mineral precipitation on the sulfur isotope composition of hydrothermal solutions. *Chemical Geology*, *105*(4), pp.259-269.